To the Graduate Council:

I am submitting herewith a thesis written by Gregory James Gosian entitled "Numerical Modeling of a 3-D Buoyancy Driven Convective Flow". I have examined the final copy of this thesis for form and content and recommend that it be accepted in partial fulfillment of the requirements for the degree of Master of Science, with a major in Engineering Science.

Basil N. Antar, Major Professor

We have read this thesis
and recommend its acceptance:

Accepted for the Council:

Associate Vice Chancellor and
Dean of the Graduate School

NUMERICAL MODELING OF A 3-D BUOYANCY DRIVEN CONVECTIVE FLOW

A Thesis
Presented for the
Master of Science
Degree
The University of Tennessee, Knoxville

Gregory James Gosian
May, 1997

for Nancy, Paris, and Betty,
the ones who raised me and told me
I could achieve whatever I wanted to,
for Berj, the one who showed me how,
and for Jacquelyn, the one who I will spend the
rest of my life with

ACKNOWLEDGMENTS

I am especially indebted to Dr. Basil Antar, my academic advisor and friend, for all he has taught me and for providing me with the opportunity to work with him. I am also grateful to him for putting up with my unusual schedule since I commuted to school from a fair distance away. I thank Dr. Farouz Sharokhi and Dr. Frank Collins as members of my review committee. I also thank Dr. John Hopkins for his assistance in learning the software used in this research, and Daniel Maxwell for writing a thesis that I used for guidance in preparing mine.

I am forever grateful to my mother, Dr. A. Nancy Avakian for being a tough act to follow and for setting the bar so high. I thank my Grandmother Paris, Grandfather Berj, my Aunt Betty (my one real Aunt) and Uncle Bill for continuous encouragement, despite the fact that my pursuits must have appeared enigmatic to them. I also thank everyone else in my family for their support and pride in my accomplishments.

Lastly, I thank Jacquelyn, for giving me the hugs, solitude, and diversions as I needed them, as well as her office, that I might finish this work so we could embark on the rest of our lives together.

ABSTRACT

The focus of this thesis is the solution of the Boussinesq approximation of the Navier-Stokes equations in order to determine the convective flow fields of an incompressible fluid in a small rectangular cuvette. The problem is a mathematical simulation of a physical problem dealing with photo deposition of a nonlinear optical crystal material from solution onto a substrate in microgravity. The temperature gradients and corresponding convective flows which arise during the photodeposition process can detrimentally influence the quality of the film deposited. An exact solution to the problem is unachievable. A finite element method was employed to solve the complete problem.The development of the method applied is given, and the results from the computations provided. It was determined that the finite element solution presented provides the information necessary to confirm the validity of the model, and accurate predictions of convective flow of similar geometry in microgravity can be made.

TABLE OF CONTENTS

CHAPTER		PAGE
1.	**Introduction**	1
2.	**Mathematical Model**	5
	The Governing Equations	5
	The Boundary Conditions	6
	Heat Sources	6
	The Physical Configuration	8
3.	**Solution Method**	10
4.	**Results and Analysis**	13
	Two Dimensional Simulations	15
	Three Dimensional Top Heating Simulations	27
	Three Dimensional Simulations with Extended Ampules	38
	Three Dimensional Side Heating Simulations	42
	Reduced Gravity Flowfield Modeling	52
5.	**Conclusion**	54
	References	56
	Appendix	59
	Vita	69

LIST OF TABLES

TABLE		PAGE
1.	Physical Parameters Used In FIDAP Input File	13
2.	MKS to CGS Conversion of Total Heat	14
3.	Heat Fluxes Used For 2-D and 3-D Models	15
4.	Maximum Velocity for Each Total Heat Top Heating 2-D - 1cm x 4cm	19
5.	Maximum Velocity for Each Total Heat Side Heating 2-D - 1cm x 4cm	19
6.	Maximum Velocity for Each Total Heat Top Heating 3-D - 1cm x 1cm x 4cm	28
7.	Ampule length and Maximum Velocities for Coarse and Fine Meshes	40
8.	Maximum Velocity for Each Total Heat Side Heating 3-D - 1cm x 1cm x 4cm	42
9.	Maximum Velocities for Each Heat for 10^{-2} g, 10^{-3} g, and 10^{-4} g	52

LIST OF FIGURES

FIGURE		PAGE
1.	3-D Geometry of Ampule	9
2.	2-D Mesh	16
3.	2-D Heating Configurations	17
4.	Velocity Vector Pattern For 2-D, 1 cm x 4 cm Geometry Area With Top Heating Through a .5 cm Wide Strip	18
5.	Plot of Total Heat vs. Maximum Velocity for 2-D 1 cm x 4 cm Geometry With Top Heating Through a .5 cm Wide Strip	21
6.	Isothermal Contours for 2-D 1 cm x 4 cm Geometry With Top Heating Through a .5 cm Wide Strip	22
7.	Velocity Vector Pattern For 2-D, 1 cm x 4 cm Geometry Area With Side Heating Through a .5 cm Wide Strip	23
8.	Plot of Total Heat vs. Maximum Velocity for 2-D 1 cm x 4 cm Geometry With Side Heating Through a .5 cm Wide Strip	24
9.	Isothermal Contours for 2-D 1 cm x 4 cm Geometry With Side Heating Through a .5 cm Wide Strip	25
10.	3-D Mesh	29
11.	3-D Top Heating Configuration	30
12.	Velocity Vector Pattern for 3-D 1 cm x 1 cm x 4 cm Top Heating Through a .5 cm Diameter Surface - plane #1	31
13.	Velocity Vector Pattern for 3-D 1 cm x 1 cm x 4 cm Top Heating Through a .5 cm Diameter Surface - plane #2	32
14.	Velocity Vector Pattern for 3-D 1 cm x 1 cm x 4 cm Top Heating Through a .5 cm Diameter Surface - plane #3	33

15.	Velocity Vector Pattern for 3-D 1 cm x 1 cm x 4 cm Top Heating Through a .5 cm Diameter Surface - plane #4	34
16.	Velocity Vector Pattern for 3-D 1 cm x 1 cm x 4 cm Top Heating Through a .5 cm Diameter Surface - plane #5	35
17.	Velocity Vector Pattern for 3-D 1 cm x 1 cm x 4 cm Top Heating Through a .5 cm Diameter Surface - overview	36
18.	Plot of Total Heat vs. Maximum Velocity for 3-D 1 cm x 1 cm x x 4 cm Geometry With Top Heating Through a .5 cm Diameter Surface	37
19.	Typical Extended Ampule 1 cm x 1 cm x 4 cm	39
20.	Plot of Maximum Velocity vs. Ampule Length, with 2-D comparison	41
21.	3-D Side Heating Configuration	43
22.	Velocity Vector Pattern for 3-D 1 cm x 1 cm x 4 cm Side Heating Through a .5 cm Diameter Surface - plane #1	44
23.	Velocity Vector Pattern for 3-D 1 cm x 1 cm x 4 cm Side Heating Through a .5 cm Diameter Surface - plane #2	45
24.	Velocity Vector Pattern for 3-D 1 cm x 1 cm x 4 cm Side Heating Through a .5 cm Diameter Surface - plane #3	46
25.	Velocity Vector Pattern for 3-D 1 cm x 1 cm x 4 cm Side Heating Through a .5 cm Diameter Surface - plane #4	47
26.	Velocity Vector Pattern for 3-D 1 cm x 1 cm x 4 cm Side Heating Through a .5 cm Diameter Surface - plane #5	48
27.	Velocity Vector Pattern for 3-D 1 cm x 1 cm x 4 cm Side Heating Through a .5 cm Diameter Surface - overview	49
28.	Plot of Total Heat vs. Maximum Velocity for 3-D 1 cm x 1 cm x x 4 cm Geometry With Side Heating Through a .5 cm Diameter Surface	50

29. Plot of Total Heat vs. Maximum Velocity for 3-D 1 cm x 1 cm x 4 cm geometry With Top Heating Through a .5 cm Diameter Surface, 1.0 g, 10^{-2} g, 10^{-3} g, and 10^{-4} g 53

1. INTRODUCTION

Almost everyone is familiar with the linear behavior of optics. They are responsible for governing the reflectivity of mirrors and the geometric laws of lenses. Less familiar are the second and third order responses of optical materials and their associated nonlinear behaviors. There are some organic polymers that are fabricated specifically to maximize nonlinear optical properties. These nonlinear optical materials can exhibit some unusual optical action. They are also of particular interest because of research currently being carried out in the field of high speed information processing, where the rise and fall times of signals is faster in these materials, by an order of magnitude, than anything currently achievable in contemporary semiconductor design (Mohlmann, 1989).

One such nonlinear optical device is the phase conjugate reflector. A beam of light (electromagnetic radiation) incident upon the phase conjugate mirror is reflected back upon itself no matter what angle any portion of the light is incident upon the reflector (Mills, 1991).

Another nonlinear device is the frequency multiplying crystal. An incident beam of light of frequency ω, passes through the crystal and emerges with a frequency of 2ω or 3ω. The energy is conserved because the emerging beam will have one half or one third the intensity of the incident beam. This is a useful phenomenon for converting infrared radiation to shorter wavelength radiation, and is employed commercially with Nd:YAG lasers. These lasers produce an internal infrared (IR)

by employing a frequency multiplying crystal, the emitted beam can be in the green portion of the visible spectrum at 527 nm (doubled) or in the ultraviolet (UV) portion at 351 nm (tripled) (Laser Focus World 1997 Buyers Guide, 1996).

Some materials which exhibit nonlinear optical behavior can also possess interesting electrical characteristics. One class of materials currently being investigated are the organic polymers, polydiacetylenes. Polydiacetylenes are of interest not only because of their nonlinear optical characteristics, but also because they are unidimensional electrical conductors and their applications in high speed computer design is being carried out in earnest (Paley et. al., 1995).

Polydiacetylenes are fabricated in the form of thin films. To be useful, the films must be of uniform thickness and defect free, otherwise optical distortion and scattering will result, or undesirable electronic characteristics will arise (Hung and Long, 1995).

To create polydiacetylene films with minimal flaws, a small chamber is filled with a solution of diacetylene monomer in 1,2 dichloroethane. One wall of the chamber is composed of an optically transparent material such as quartz. As the solution is irradiated through the quartz with monochromatic ultraviolet (UV) light, a photo-polymerization reaction occurs and a thin polydiacetylene film is deposited on the inside surface of the quartz substrate. The thickness of the film is determined by the intensity of the radiation and the duration of the exposure (Paley et. al., 1995).

However, the film and the monomer solution generate heat due to the absorption of the UV radiation. The result is that the solution at the top of the chamber

is hotter than the solution farther down, not only from absorption of the UV energy by the solution, but also by conduction of heat from the film itself. With the sides and bottom of the chamber being held at fixed temperature, this leads to an uneven distribution of heat, and hence, temperature gradients arise, along with corresponding density variations. The density gradients, under the influence of gravity, induce a buoyancy driven convective flow. Understanding the nature of the flow is important for two reasons (Paley et. al., 1995).

First, polymer chains in the bulk solution collide and coalesce to form solid particles a few hundredths of a micron in size, due to the convection. These particles are so small, they do not readily sediment out of solution and thus remain suspended. Convection further transports these particles to the surface of the growing film, where they could become imbedded. These particles act as defects and cause undesirable characteristics in the film (Paley et. al., 1995).

Second, evidence suggests that convection can have a detrimental effect on the molecular alignment and orientation of the polymer chains in the film. Well oriented polydiacetylene films are capable of greater optical nonlinearity and better unidimensional electronic conductivity than poorly oriented films are (Paley et. al., 1995).

All of these convective effects can be greatly minimized by carrying out the fabrication process in a micro-gravity environment, either on the space shuttle or a space station. By numerically modeling the convective flows in an Earth normal 1-g (g

is the acceleration due to gravity 981 cm/sec^2) environment, and comparing the results with data gathered empirically in a Earth based 1-g laboratory, the validity of the numerical model can be ascertained. A valid prediction of fluid behavior in a micro-gravity environment can then be made, and parameters be adjusted to minimize convective effects before the process is carried out in micro-gravity.

2. MATHEMATICAL MODEL

THE GOVERNING EQUATIONS

The goal of this reaseach is to describe the velocity vector field of a three dimensional (3-D) simulated convective flow of an incompressible fluid. To do so, it is necessary to solve the Navier-Stokes equations for the problem. These are given as, for this buoyancy driven convective flow problem, the conservation of mass equation:

$$\frac{\partial u_i}{\partial x_i} = 0 \qquad [1]$$

the energy equation:

$$\frac{\partial T}{\partial t} + u_j \frac{\partial T}{\partial x_j} = \frac{k}{\rho c_v} \frac{\partial^2 T}{\partial x_j \partial x_j} \qquad [2]$$

and the Bousinessq approximation to the momentum equation:

$$\frac{\partial u_i}{\partial t} + u_j \frac{\partial u_i}{\partial x_j} = -\frac{1}{\rho} \frac{\partial p}{\partial x_i} + \frac{\mu}{\rho} \frac{\partial^2 u_i}{\partial x_j \partial x_j} + g_i \beta (T - T_\infty) \qquad [3]$$

(Antar, 1995), where the following notations are used:

x_i = i th component of position
u_i = i th component of velocity
g_i = i th component of gravitational acceleration
ρ = density
μ = viscosity
c_v = specific heat

k = heat conductivity
β = volume expansion coefficient
T = local temperature
T_∞ = temperature at an infinite distance away (in actuality, a reference temperature)
Q = heat input through the flux area
n = normal direction

THE BOUNDARY CONDITIONS

Equations [1], [2], and [3] must be solved subject to the no-slip boundary condition on all solid surfaces,

$$u_{i_{wall}} = 0 \qquad [4]$$

and the appropriate thermal conditions at each surface:

$$T = T_{wall} \qquad [5]$$

or

$$\frac{\partial T}{\partial n} = 0 \qquad [6]$$

These thermal boundary conditions describe a constant temperature and no heat flux everywhere on the wall, except at locations where there exists a heat flux into the system. At these locations, the heat flux is given by:

$$\frac{\partial T}{\partial n} = Q \qquad [7]$$

HEAT SOURCES

As stated earlier, both the nonlinear film being deposited on the substrate and the solution itself generate heat due to the absorption of UV radiation. These represent

the major sources of heat in the system. The heat generated by polymerization process is minor due to only a small fraction of the monomer in solution actually having reacted, and this over the period of the UV exposure. The solution to the transport equation for the UV intensity through an attenuating medium $\frac{dI}{dx} = -\varepsilon_f I$ (Tipler, 1982) leads to an expression for the heat generated, Q_1, by the film (on the inside of the substrate wall), and is given by:

$$Q_1 = I_0(1-e^{-\varepsilon_f l}) \qquad [8]$$

where I_0 is the intensity of the UV source, ε_f is the absorption coefficient of the film, and l is the thickness of the film. The heat, Q_2, generated by the absorption of the remaining UV radiation by the solution across a depth d, is given by:

$$Q_2 = I_{00}(1-e^{-\varepsilon_s d}) = I_0 e^{-\varepsilon_f l}(1-e^{-\varepsilon_s d}) \qquad [9]$$

where ε_s is the absorption coefficient of the monomer solution which is typically 150 cm^{-1} for the solution utilized here (Paley et. al., 1995). This implies that nearly all of the UV radiation is absorbed in the first 50 μm of depth, either by the film or the solution itself. There is essentially no energy absorbed by the quartz at all. This leads to a simplification for the computational model in which the UV radiation may be very well approximated by a heat flux across the top (or side) area representing the location of where the UV radiation penetrates the boundary wall (Cember, 1969).

THE PHYSICAL CONFIGURATION

Solutions to the 3-D problems are to be determined. These are the simulations that describe the actual physical problems, using a defined volume of 1 cm x 1 cm x 4 cm, corresponding to the real ampule dimensions used in fabricating the optical film. The area of the heat flux is set in all simulations as a .5 cm diameter circular area centered on top of the ampule for one set of trials (corresponding to a .5 cm diameter UV laser beam through a quartz window comprising the top), and a .5 cm diameter circular area centered on one of the sides for another set of trials (corresponding to a .5 cm diameter UV laser beam through a quartz window comprising the side), as illustrated in Figure 1. Heat inputs of .25, .50, 1.00, 1.50, 2.00, 4.00 Watts are investigated for each case of top and side heating. A 1g gravity vector downward is defined for these sets of trials. This is in order to produce results which could be compared with data gathered experimentally under terrestrial conditions.

Another set of trials using 10^{-2}, 10^{-3}, and 10^{-4} g gravity vectors pointing downward are defined for each of a set of trials utilizing each of the six heat fluxes through the top. This is to be able to provide predictive data for when the ampules and the production apparatus are to be used on future space flights in a reduced gravity environment.

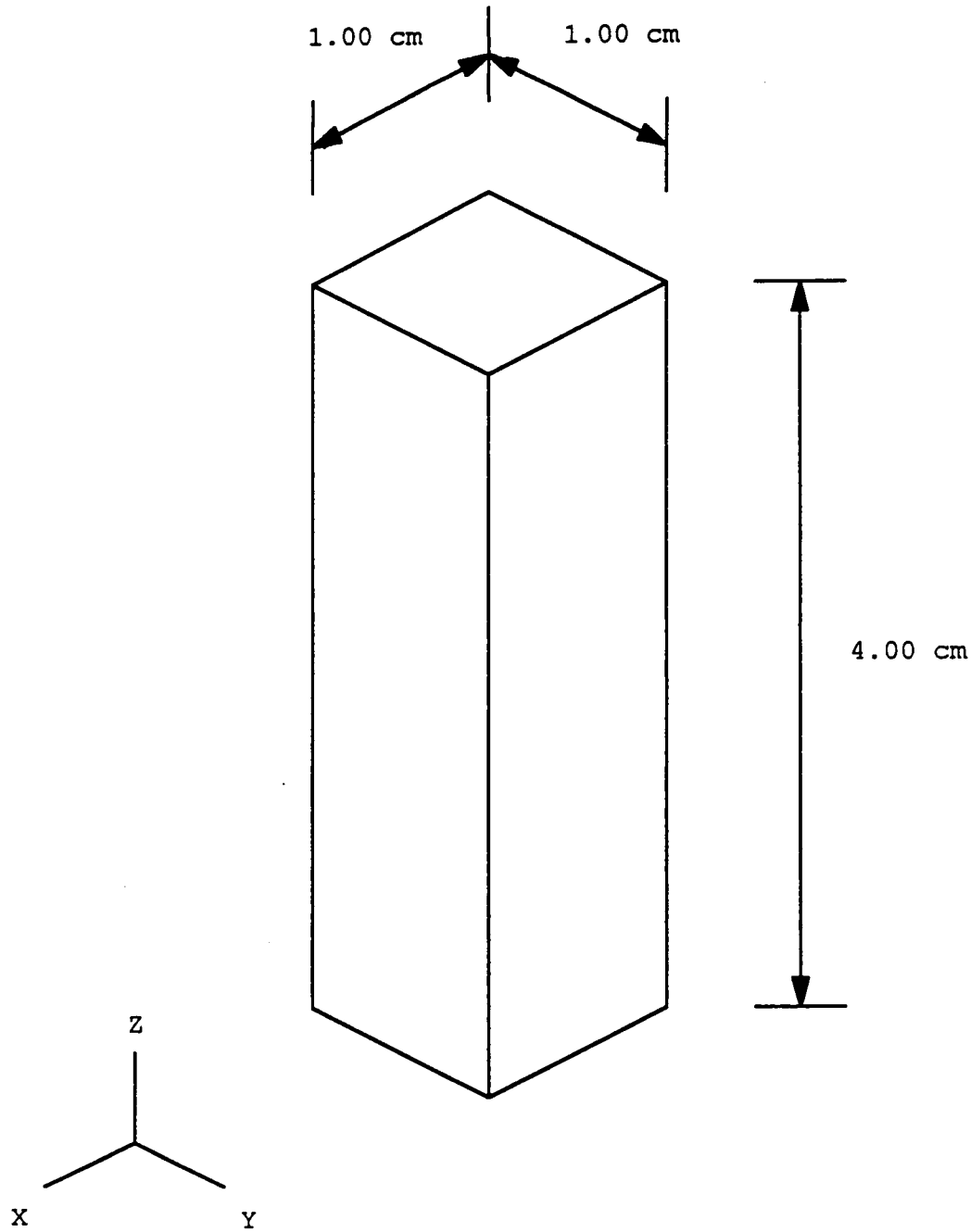


Figure 1. 3-D Geometry of Ampule

3. SOLUTION METHOD

There is no closed form solution to the Navier-Stokes equations, [1] - [3], governing a convective flow under the conditions specified by the mathematical model of the previous chapter. Therefore, a numerical approach to produce an approximation to the solution must be undertaken. This research utilized a commercially available computational fluid dynamics (CFD) program designed to numerically solve the Navier-Stokes equations using the finite element method. The program is called FIDAP which is an acronym for *Flu*id *D*ynamics *A*nalysis *P*ackage, version 7.52 available from Fluid Dynamics International. The program was run on the University of Tennessee Space Institute's Sun MicroSystem SPARC2000 computer.

The computer program FIDAP is very flexible in that it allows for a problem with its associated geometry and finite element analysis mesh to be defined once, and then with some very slight changes in the instruction set, parameters of the problem (boundary conditions, mesh density, solution convergence conditions) can be altered and the trials rerun, without the cumbersome need for rewriting sections of a created-from-scratch computer code. It is actually composed of a number of subprograms, each dedicated to a specific task.

Dividing the computational region into a number of discrete cells or finite elements is a procedure called "meshing". Meshing of a geometric region takes place automatically in FIDAP in a subprogram called FIMESH, and the procedure is relatively straightforward. The region is first defined in a geometric real space, as well

as in a FIDAP utilized Integer Space. The geometric real space corresponds to the physical problem and its region. The Integer Space is where the region exists numerically, along with its prominent features: corners, edges, boundary surfaces, heating surfaces, etc. It is within the FIMESH subprogram that parameters such as the number of nodal points along the edges, finite element unit geometries, and labeling assignments for the boundaries, heating surfaces, and fluid areas take place (FIDAP 7.0, FIMESH Users Manual, 1993).

A second subprogram, FIPREP, is where all of the values of the physical parameters are specified or prepared. These include the fluid's specific heat, viscosity, volume expansion coefficient, thermal conductivity coefficient, density, and the local gravity vector. The convergence conditions are also defined in this subprogram, as well as the boundary conditions (FIDAP 7.0, FIPREP Users Manual, 1993).

FIDAP is the main command program in the CFD package, and is run in Graphical User Interface (GUI) mode. This is an icon driven real time interface program. To start a FIDAP simulation run, a source file is first created in a text editor, and stored. It describes the problem type, its geometry and initial and/or boundary conditions. It is read by the GUI section of the command program. As the source file is read, FIDAP first invokes FIMESH. This subprogram checks the relevant sections of the source file for syntax and completeness, and when each is satisfied, it returns control back to the main command program. FIPREP is then invoked, and the reading of the source file continues with this subprogram. After FIPREP checks the source file

it returns control back to the FIDAP command program. The command program runs a number of routines and node numbering algorithms to make the simulation execute as efficiently as possible. When FIDAP is satisfied as to the successful creation of parameters needed for a simulation to be run, it states as much and waits for operator input to commence solving the simulation (FIDAP 7.0, Tutorial Manual, 1993).

When the solution reaches convergence, the simulation run is terminated. A third subprogram, FIPOST, is then invoked under operator command, to perform the post processing analysis. FIPOST is where the plots for temperature and streamline contours, velocity vectors, and mesh displays are made. All of the display controls allowing for pan, zoom and rotation are available. Results are displayed on the work station monitor, or can be directed to any of a number of output devices, printers, plotters, or files (FIDAP 7.0, FIPOST Users Manual, 1993).

A complete listing of the FIDAP input files which describe the particular problem being executed (2-D or 3-D), along with comments describing what the relevant lines of code are being processed into, can be found later in Appendix A.

Finally, the simulations had the option to be run dimensionalized or non dimensionalized. Leaving the problem in dimensional form was chosen. This had two advantages. First, real world velocities were generated, and this allowed for the inspection of intermediate results as the simulations were being run. Second, it avoided two extra steps of non dimensionalizing the problem at the start of the simulation, and dimensionalizing the result.

4. RESULTS and ANALYSIS

The numerical solution to the problem was carried out in stages. First, the solutions to the corresponding 2-D problems were attempted. This had the advantage of allowing familiarity with the extensive programming capabilities of the FIDAP package to be gained. Since the problem was one of relatively simple geometry, it also allowed for quick simulation runs during the learning process of the software. Convergence and steady state solution could be achieved in about seven minutes per simulation.

The FIDAP program would run dimensionalized problems in the CGS (centimeter, gram, seconds) system of measurement and certain physical parameters of the fluid were consistent in all of the trials, as outlined in Table 1.

These are the physical properties of water at 25 ^{0}C, which is the fluid model used in this analysis. Water was the fluid investigated experimentally, and it is close

Table 1. Physical Parameters Used In FIDAP Input Files
(Handbook of Chemistry and Physics, 1994-1995)

Specific Heat	.99828 cal/gm-^{0}K
Viscosity	.008904 Poise
Volume Expansion Coefficient	1.1204 x 10^{-4} /^{0}K
Heat Conductivity	.0014503 cal/cm-sec-^{0}K
Density	.99705 gm/cm^{3}

enough in behavior to a solution of diacetylene monomer in 1,2 dichloroethane to provide an approximation of that fluid's behavior also.

Choosing to run the simulations dimensionally requires that careful attention be paid to the units associated with the physical constants employed. Heat is commonly specified in units of Watts and the CGS system FIDAP utilizes needs heat to be specified in CGS units of cal/sec. This yielded the heat conversions shown in Table 2.

Further, since the FIDAP program utilizes heat flux rather than total heat, the CGS total heat inputs must be divided by the area representing the UV laser illumination. Table 3 shows CGS total heat inputs divided by area, yielding heat fluxes to be utilized in the simulation input files. The total heat inputs are divided by .5 cm for the 2-D cases, representing a .5 cm wide flux strip. They are also divided by .1963 cm^2 (to be used later in investigation of the 3-D cases), representing a .5 cm diameter circular flux area.

Table 2. MKS to CGS Conversion of Total Heat

CGS Total Heat Input (cal/sec)	MKS Total Heat Input (watts)
.0597	.25
.1195	.50
.2389	1.00
.3584	1.50
.4778	2.00
.9556	4.00

Table 3. Heat Fluxes Used For 2-D and 3-D Models

CGS Total Heat Input (cal/sec)	2-D heat flux (cal/sec-cm)	3-D heat flux ($cal/sec\text{-}cm^2$)
.0597	.1195	.3042
.1195	.2389	.6084
.2389	.4778	1.2168
.3584	.7168	1.8252
.4778	.9556	2.4336
.9556	1.9112	4.8672

TWO-DIMENSIONAL SIMULATIONS

The 2-D simulations were carried out utilizing a mesh of 24 by 24 elements as shown in figure 2. A physical region measuring 1 cm wide x 4 cm high was used. Heat inputs of .25, .50, 1.00, 1.50, 2.00, and 4.00 watts were investigated with the flux through a .5 cm wide one dimensional (since this is a 2-D problem) surface. The heated surface was centered on top for one set of trials with each of the six heat fluxes, and centered on the side for another set of trials, as illustrated in Figure 3. A 1-g gravity vector downward was defined for all cases.

The first set of trials investigated the six different heat inputs utilizing heating from the top. The velocity vector patterns generated for each of the trials were identical to each other as represented by the 1.00 watt trial shown in Figure 4. The maximum velocity for each trial (and correspondingly all values of the velocity throughout the

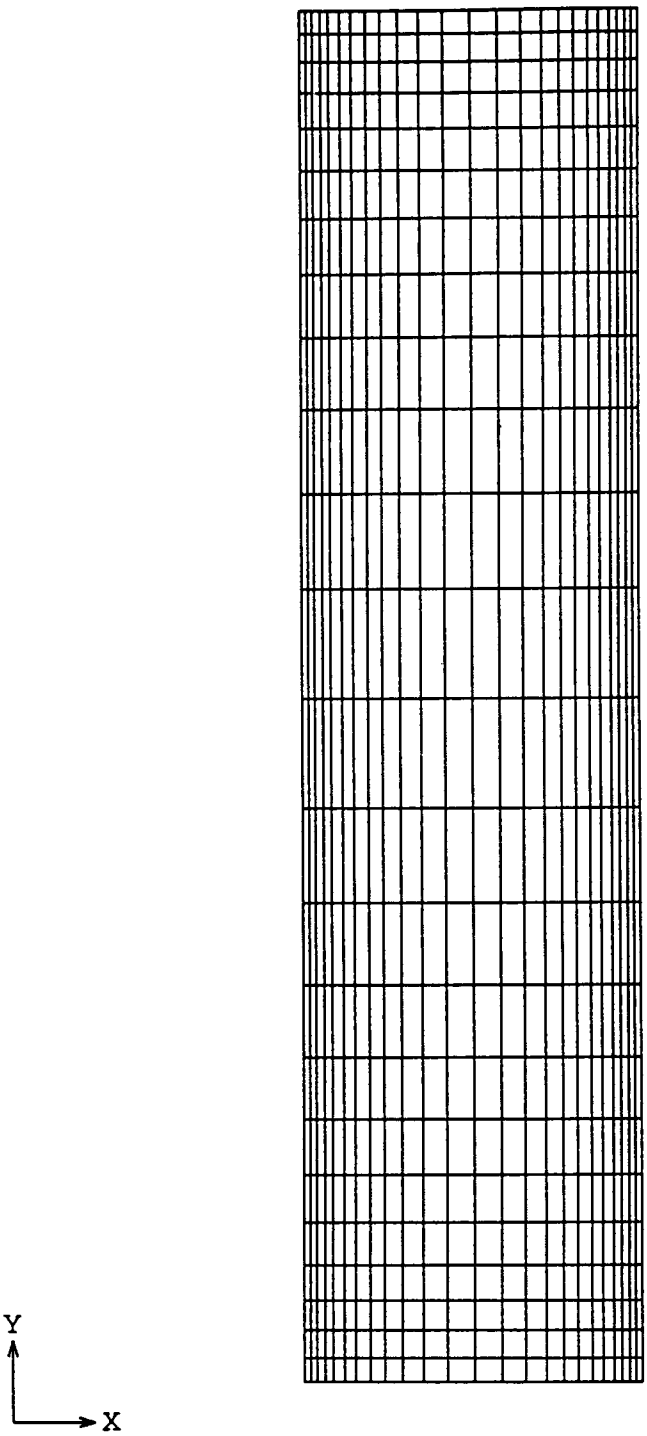


Figure 2. 2-D Mesh

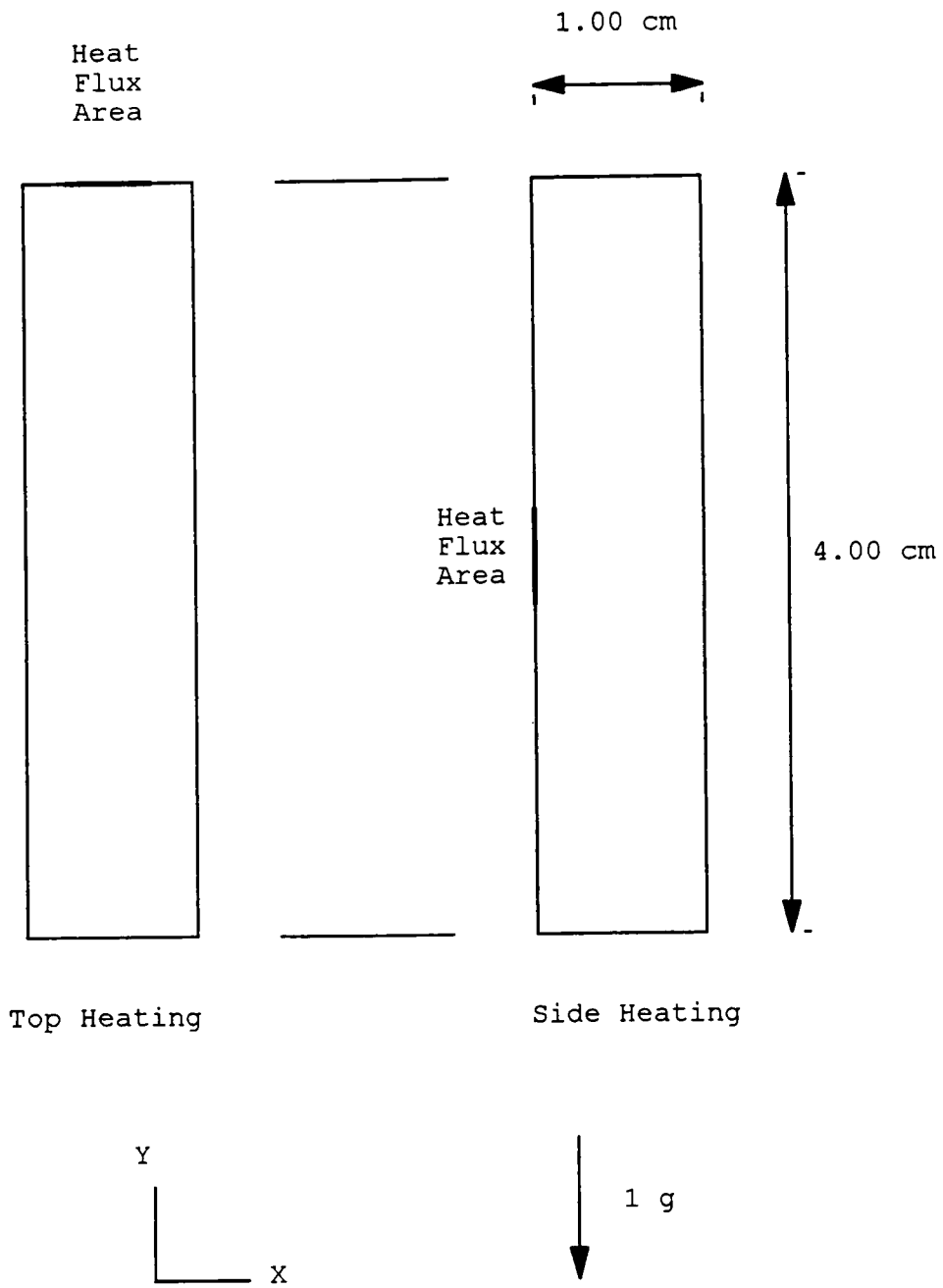


Figure 3. 2-D Heating Configurations

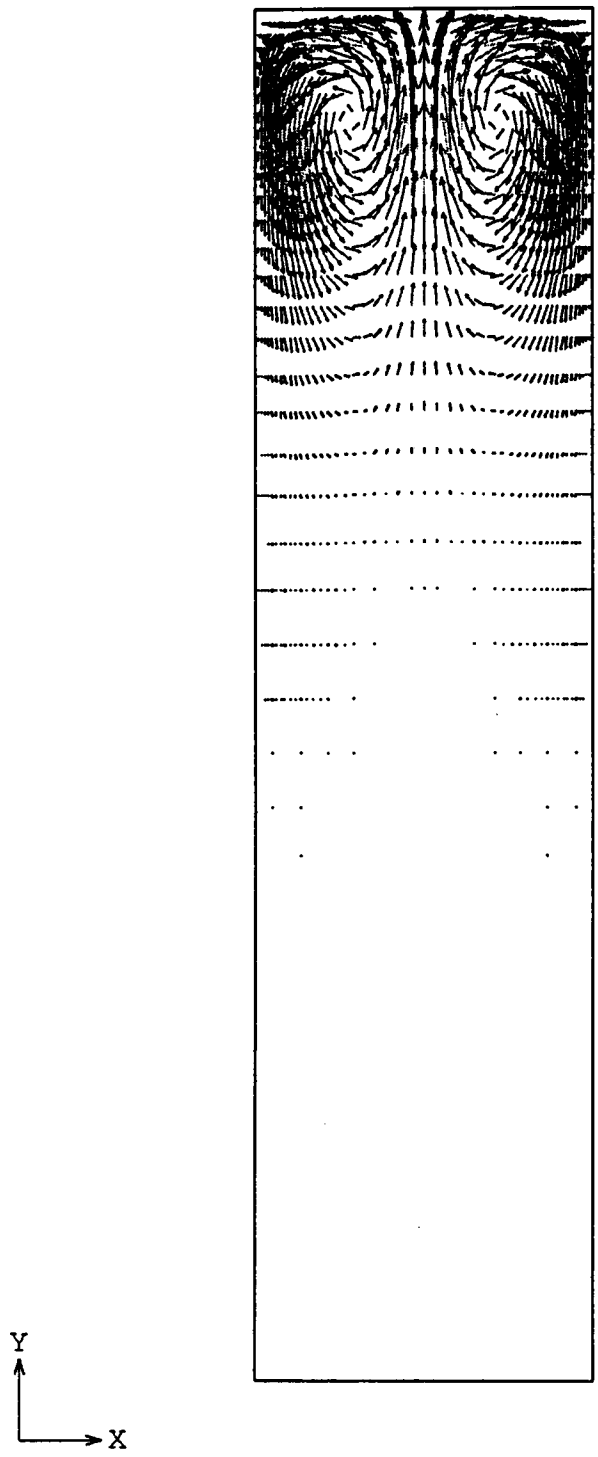


Figure 4. Velocity Vector Pattern For 2-D, 1 cm x 4 cm Geometry With Top Heating Through a .5 cm Wide Strip

mesh) varied linearly with the heat input. Investigating the maximum velocity generated in the flow field is a useful scale to parameterize all of the flows by (2-D and 3-D). The maximum velocity for each total heat value is shown in Table 4 and plotted in Figure 5.

Isothermal contours are shown in Figure 6, but even in the case of 4.00 watt total heat input, the maximum temperature just inside the heat flux area is only 25.5 ^{0}C, and drops off to 25 ^{0}C, the wall temperature, rather quickly.

Using the same mesh, the next set of trials investigated the six different heat inputs utilizing heating from the side. The velocity vector patterns generated for each of these trials were identical to each other as represented by the 1.00 watt trial shown in Figure 7 and the flow fields are identical to each other except in scale (which again varied linearly with heat input). The velocity vector pattern generated for each of the trials is represented by Figure 7. The maximum velocity for each total heat is shown below in Table 5, and plotted in Figure 8.

Isothermal contours are shown in Figure 9, but again, in the case of 4.00 watt total heat input, the maximum temperature just inside the heat flux area is only 25.5 ^{0}C, and drops off to 25 ^{0}C, the wall temperature and the rest of the fluid bulk temperature.

The convective patterns of the 2-D flows have the expected appearance (see Figures 4 and 7) and the velocities of the flows have reasonable values (see Tables 4 and 5). The data also shows that the velocities generated in the ampule are approximately four and one half times greater in the case of side heating than with top

Table 4. Maximum Velocity for Each Total Heat
Top Heating 2-D - 1 cm x 4 cm

Total Heat (watts)	Maximum velocity (cm/sec)
.25	3.768×10^{-4}
.50	7.533×10^{-4}
1.00	1.506×10^{-3}
1.50	2.259×10^{-3}
2.00	3.011×10^{-3}
4.00	6.016×10^{-3}

Table 5. Maximum Velocity for Each Total Heat
Side Heating 2-D - 1 cm x 4 cm

Total Heat (watts)	Maximum velocity (cm/sec)
.25	1.772×10^{-3}
.50	3.542×10^{-3}
1.00	7.084×10^{-3}
1.50	1.060×10^{-2}
2.00	1.420×10^{-2}
4.00	2.830×10^{-2}

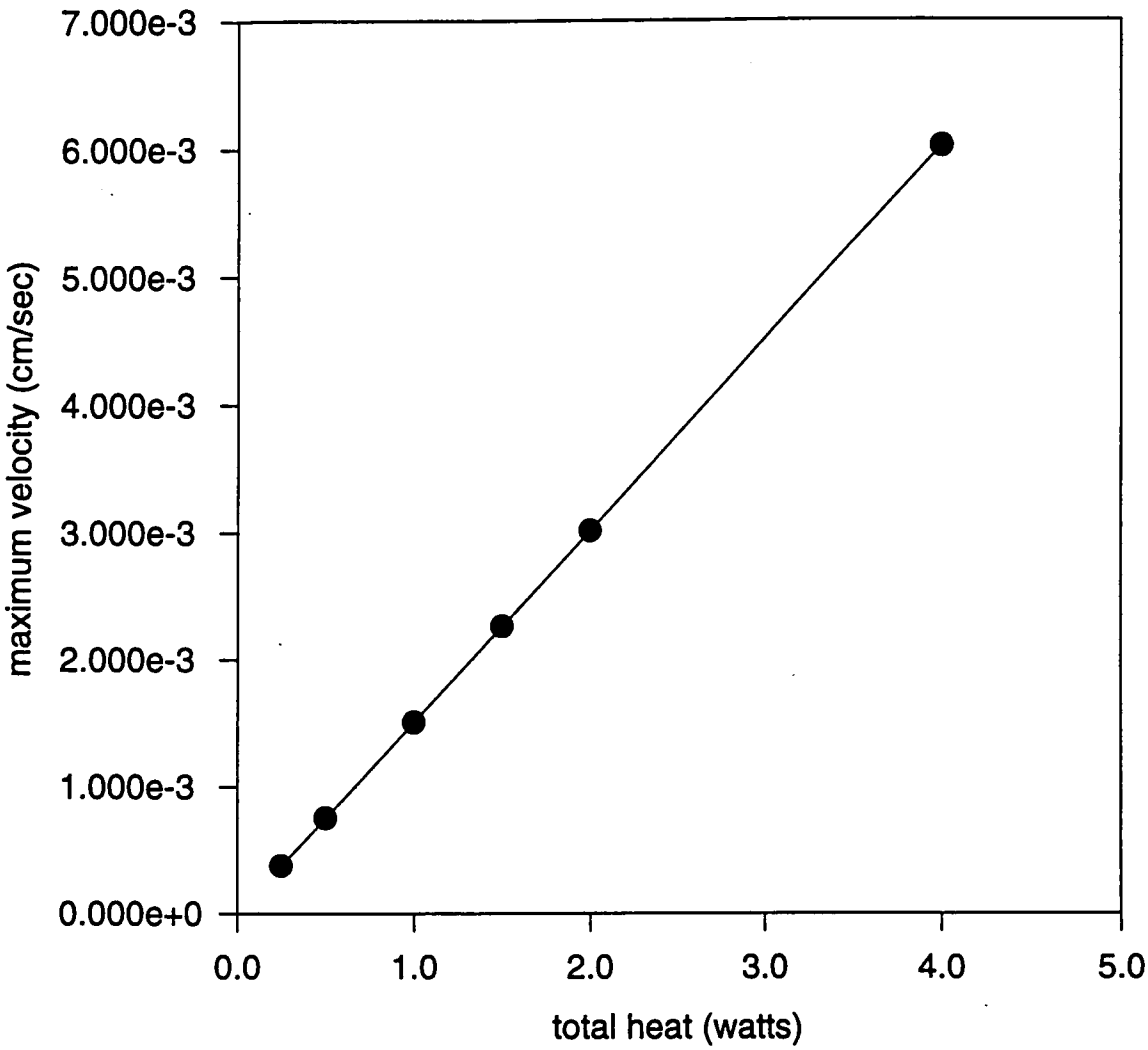


Figure 5. Plot of Total Heat vs. Maximum Velocity for 2-D 1 cm x 4 cm Geometry With Top Heating Through a .5 cm Wide Strip

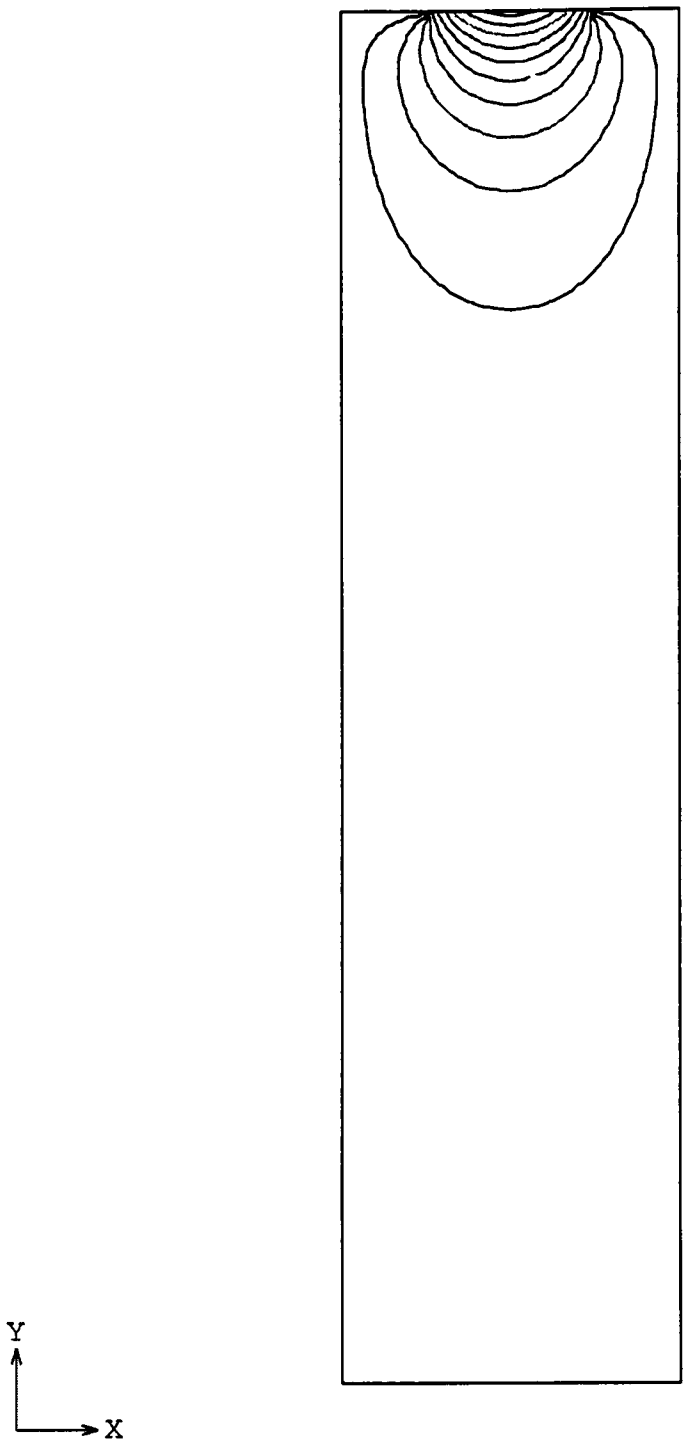


Figure 6. Isothermal Contours for 2-D 1 cm x 4 cm Geometry With Top Heating Through a .5 cm Wide Strip

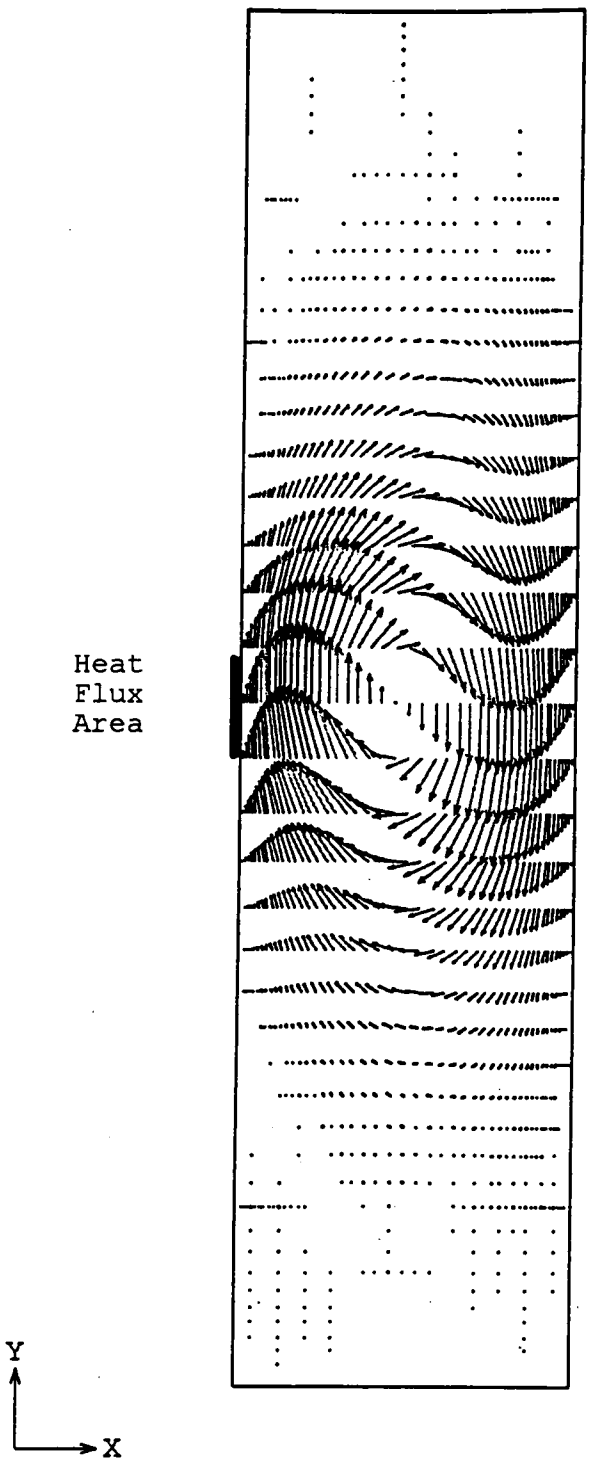


Figure 7. Velocity Vector Pattern For 2-D 1 cm x 4 cm Geometry With Side Heating Through a .5 cm Wide Strip

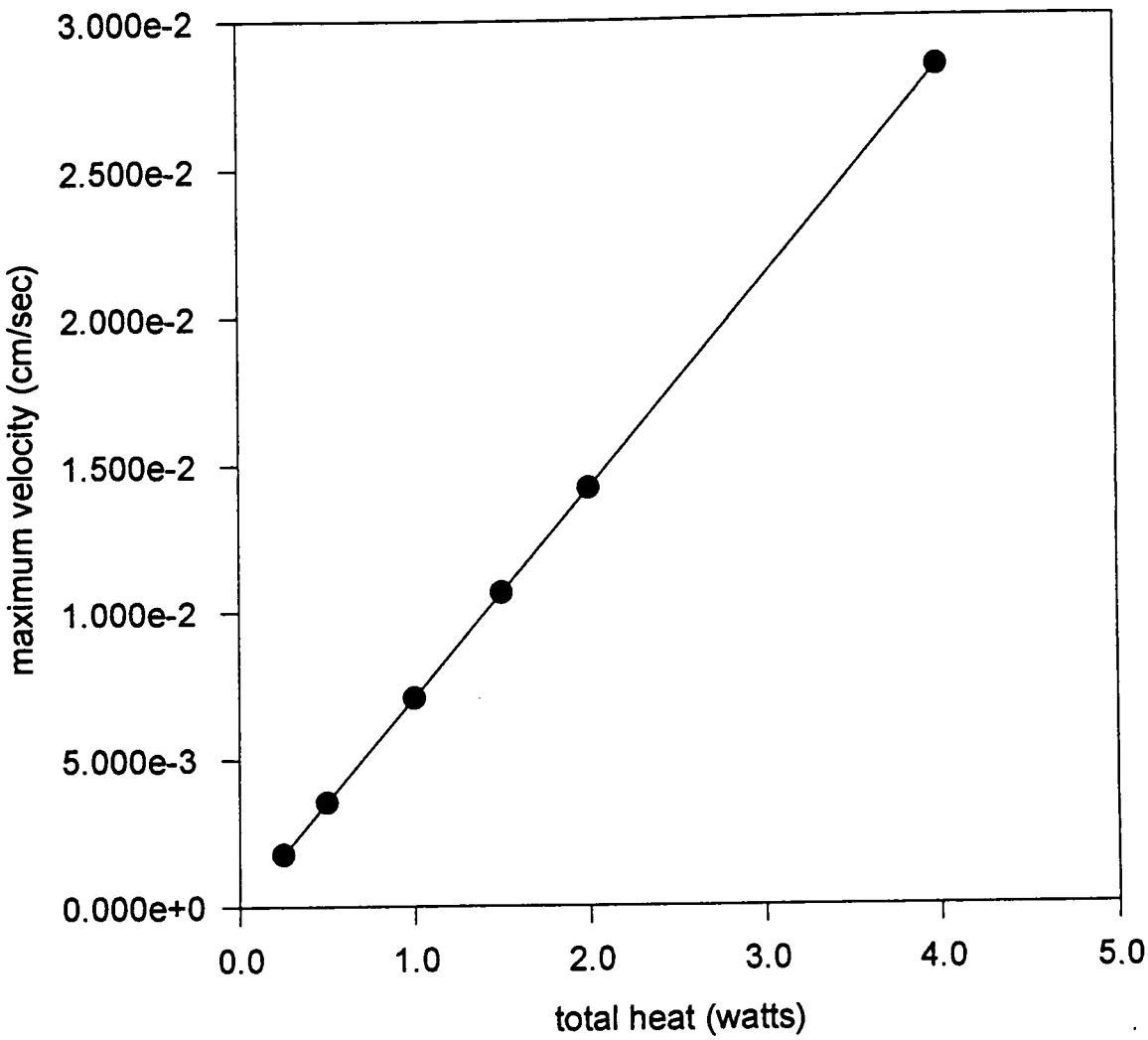


Figure 8. Plot of Total Heat vs. Maximum Velocity for 2-D 1 cm x 4 cm Geometry With Side Heating Through a .5 cm Wide Strip

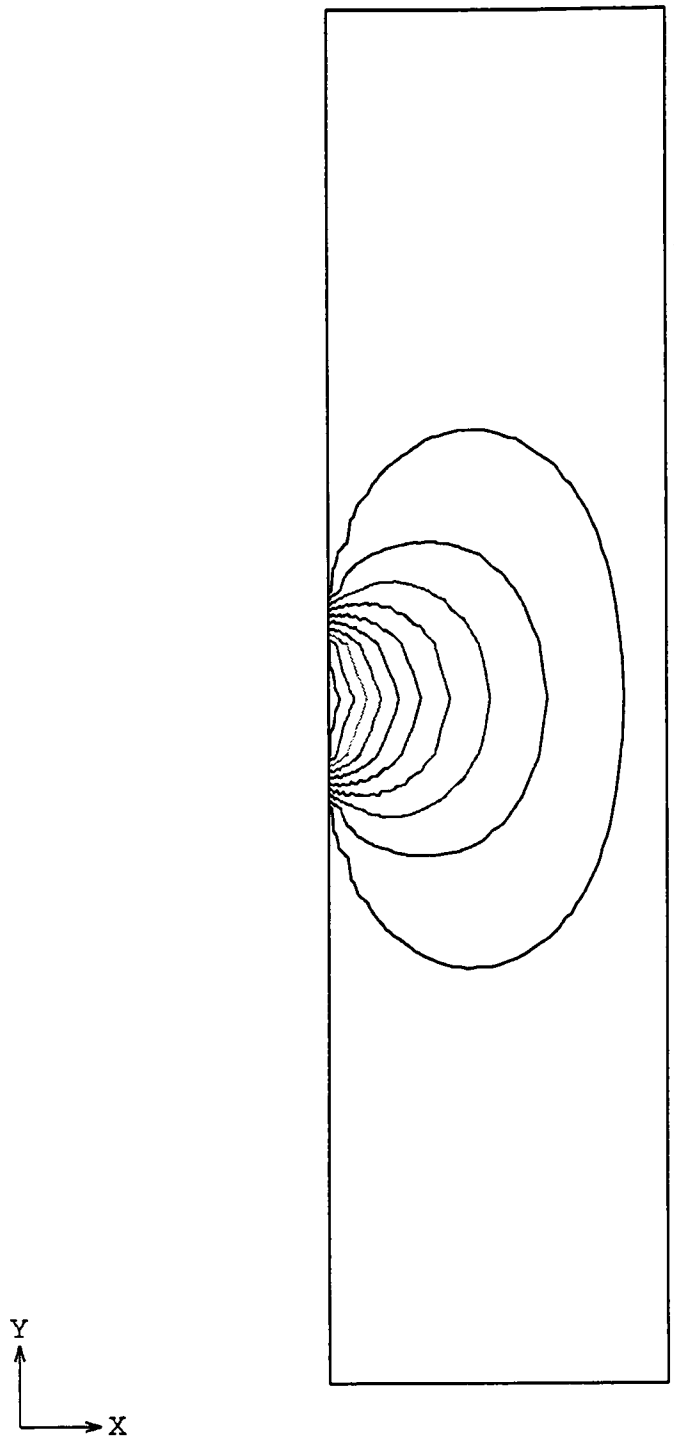


Figure 9. Isothermal Contours for 2-D 1 cm x 4 cm Geometry With Side Heating Through a .5 cm Wide Strip

heating. This is consistent with what we already know of convective flows; the location of the heating surface on the side generates a more convectively unstable density.

The maximum velocity occurs in the same place for all cases of top heating, at X = .50 cm, Y = 3.72 cm. The maximum velocity occurs in the same place for all cases of side heating, at X = .15 cm, Y = 2.00 cm.

THREE-DIMENSIONAL TOP HEATING SIMULATIONS

These 3-D simulations were carried out utilizing a mesh of 13 elements high by 12 elements wide by 12 elements long. The 3-D simulations utilized a mesh not as fine along any one dimensional edge as in the 2-D cases because of the memory limitations of the computational facility. Though this results in slightly greater inaccuracies in the solutions, simulations carried out in 2-D with a 12 element by 12 element mesh (comparable to this 3-D mesh), and the finer 24 element by 24 element mesh presented in the previous section, showed a greater than 97% agreement in velocities calculated throughout the flows. This led to the determination that the solutions calculated in 3-D with this particular mesh would be quite acceptable.

The finite element mesh is shown in Figure 10, and the heating geometry in Figure 11. Fine element resolution on the bottom of the ampule was deemed unnecessary because results from the 2-D cases indicated that hardly any fluid circulation was occurring at the bottom,even a moderate distance above the bottom surface. The heat inputs were .25, .50, 1.00, 1.50, 2.00, and 4.00 watts.

Six trials investigated the six different heats utilizing heating from the top. The maximum velocity for each total heat is shown in Table 6. The velocity vector patterns generated for each of the trials were identical to each other as represented by the cross sectional planes shown in Figures 12 through 17. The maximum velocity for each total heat is plotted in Figure 18. Of interest to note is the bilateral symmetry of the flow across the x-direction median, and the y-direction median for this case.

Table 6. Maximum Velocity for Each Total Heat
Top Heating 3-D - 1 cm x 1 cm x 4 cm

Total Heat (watts)	Maximum velocity (cm/sec)
.25	1.419×10^{-3}
.50	2.835×10^{-3}
1.00	5.661×10^{-3}
1.50	8.479×10^{-3}
2.00	1.129×10^{-2}
4.00	2.243×10^{-2}

The convective patterns of the 3-D flows have the appearance expected based on the 2-D flow patterns previously determined, and the velocities of the flows have reasonable values. A cursory investigation of the 3-D top heating velocities show that they are roughly 3.75 times greater in magnitude than the 2-D top heating velocities. This could be accounted for by the fact that, while total heats in both the 2-D and 3-D cases are the same (trial for trial), the flux density of the 3-D cases is greater than the flux density for the 2-D cases (trial by trial) by about two and a half times. This variation in flux density is due to the differing areas each heat input flows through in the 2-D and 3-D cases. This leads to increased localized heating in 3-D trials, and correspondingly steeper density gradients, therefore maximum velocities are expected to be higher in the 3-D cases. This suggested an interesting aside experiment which would go further in confirming confidence in the numerical model.

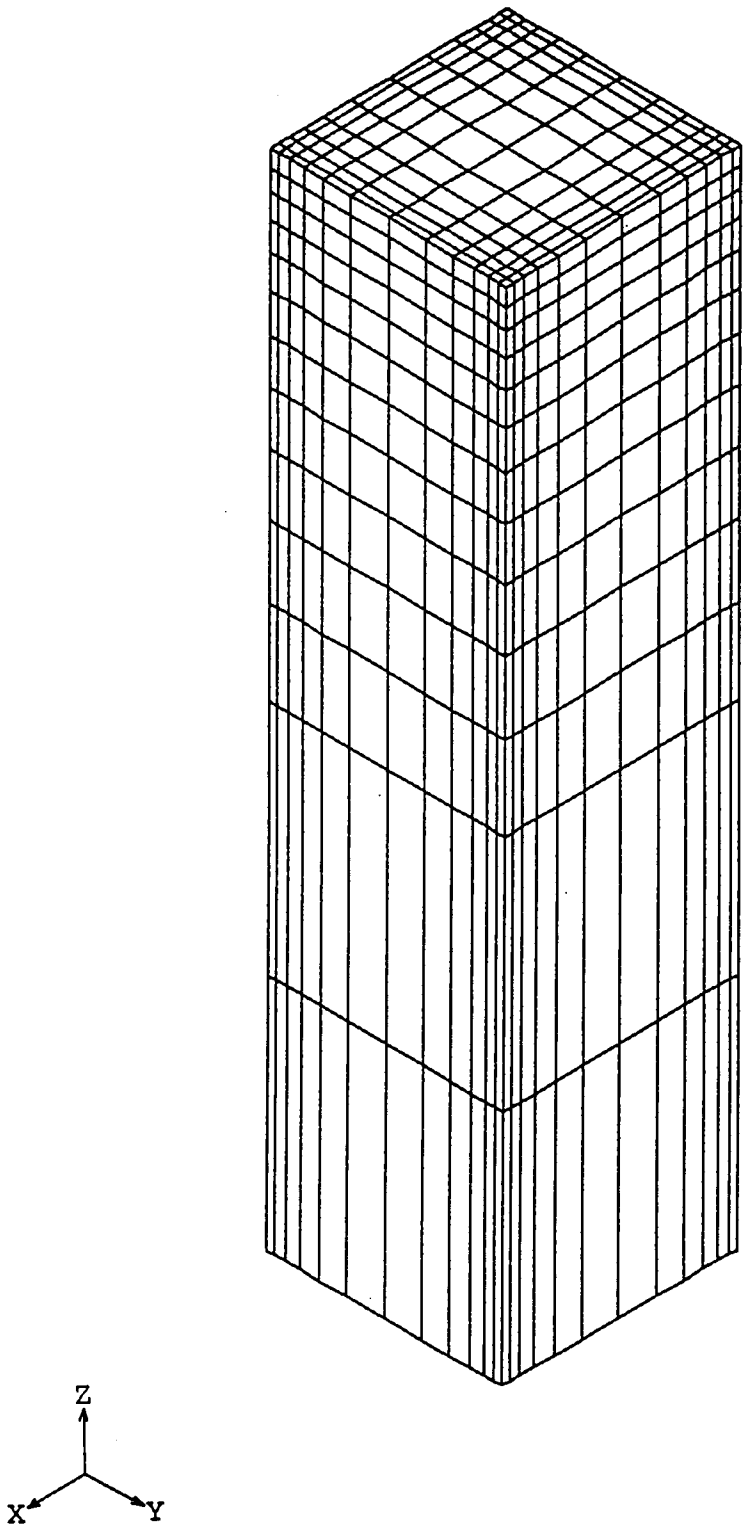


Figure 10. 3-D Mesh

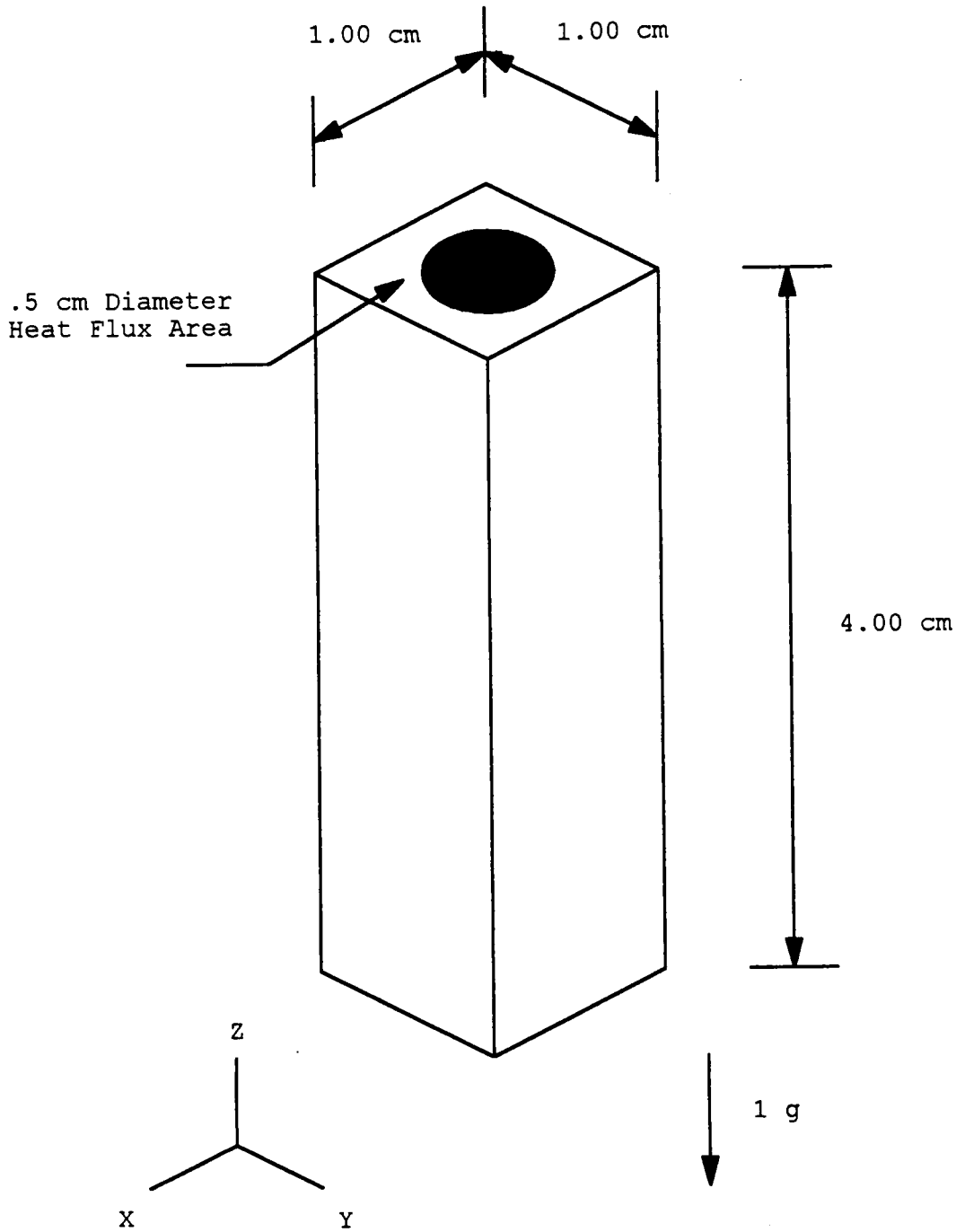


Figure 11. 3-D Top Heating Configuration

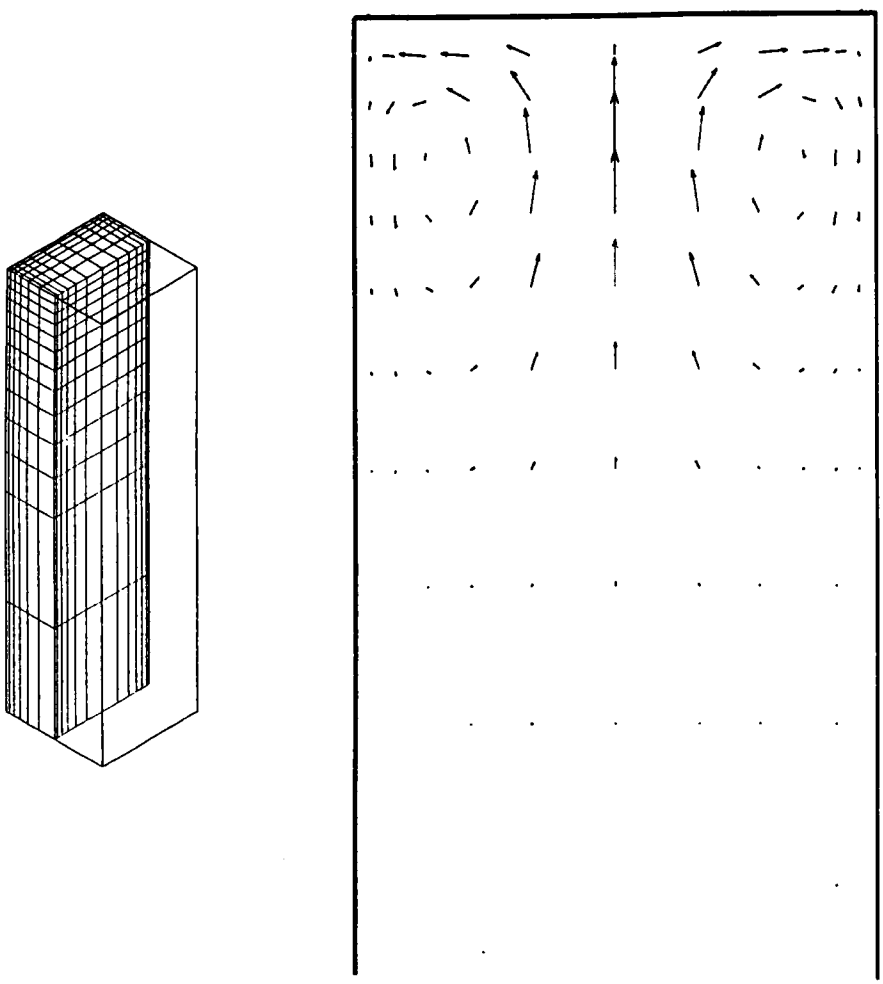


Figure 12. Velocity Vector Pattern For 3-D 1 cm x 1 cm x 4 cm Top Heating Through a .5 cm Diameter Surface - plane #1

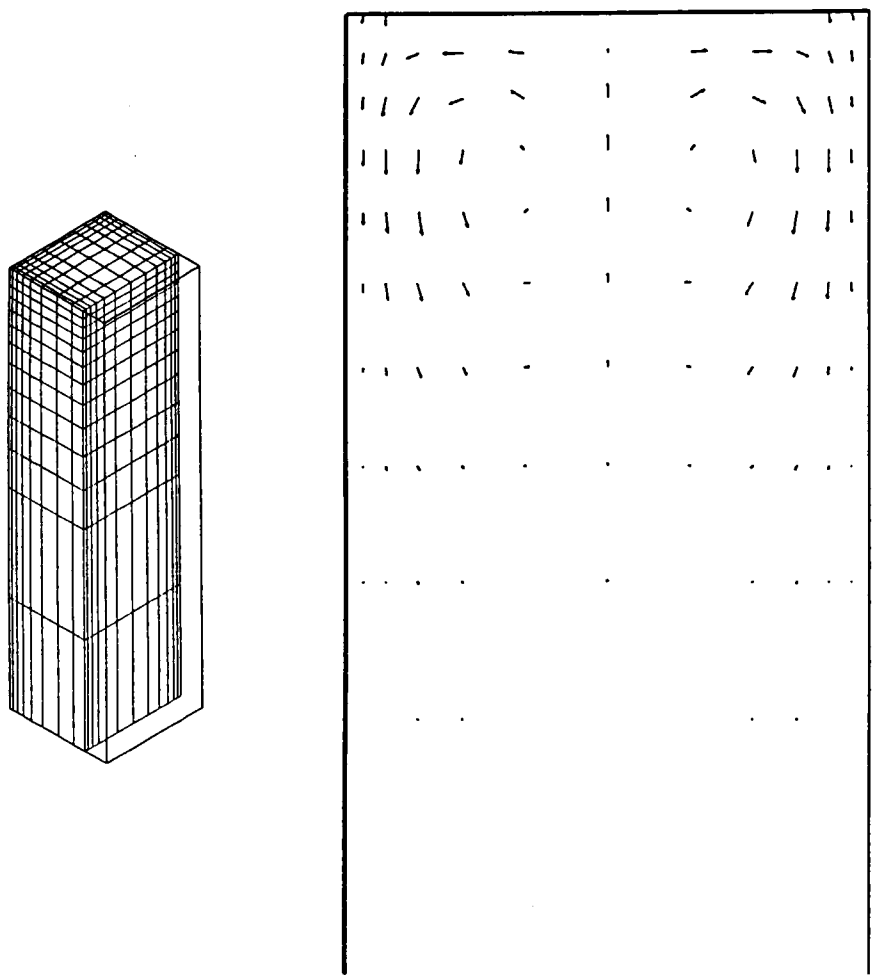


Figure 13. Velocity Vector Pattern For 3-D 1 cm x 1 cm x 4 cm Top Heating Through a .5 cm Diameter Surface - plane #2

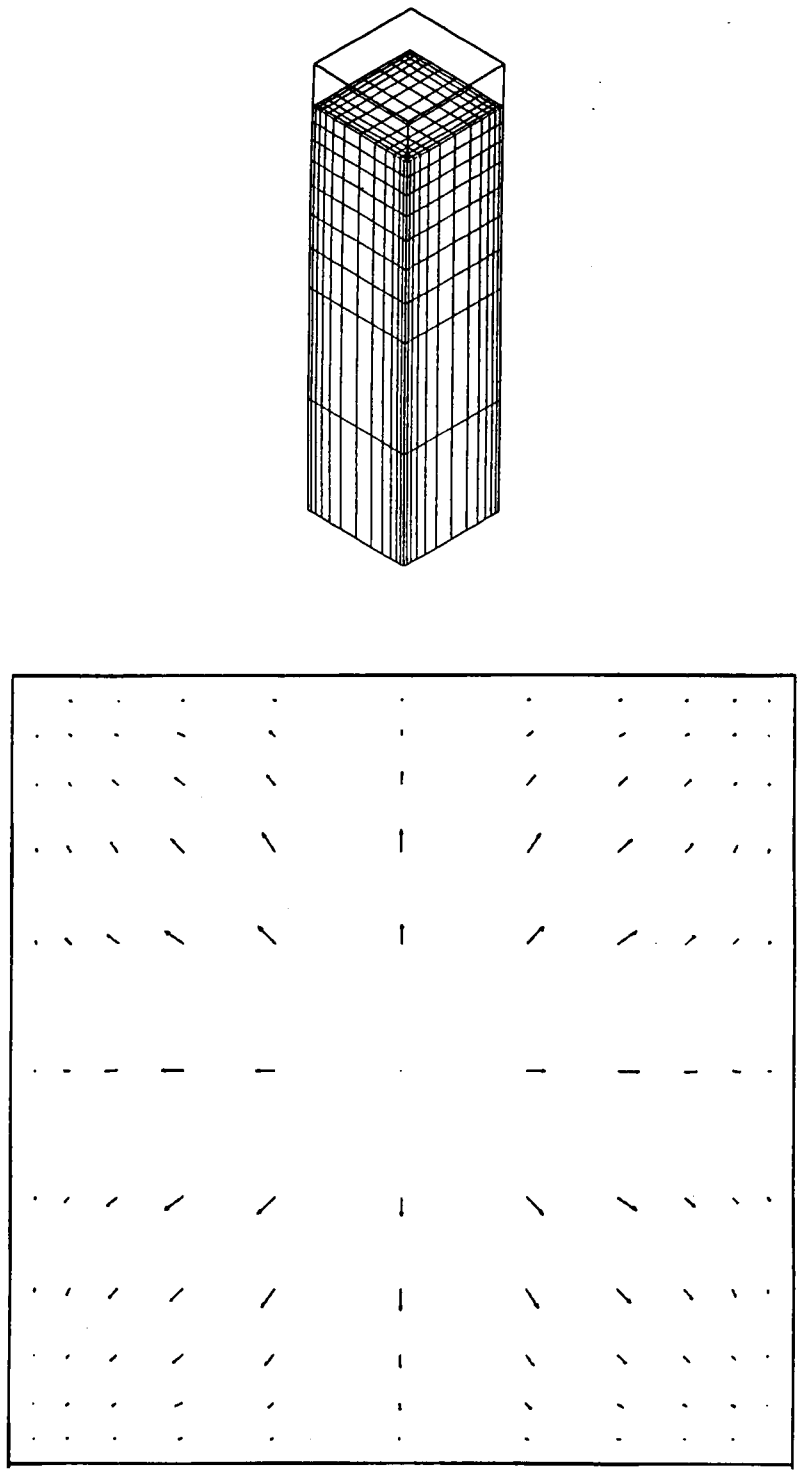


Figure 14. Velocity Vector Pattern For 3-D 1 cm x 1 cm x 4 cm Top Heating Through a .5 cm Diameter Surface - plane #3

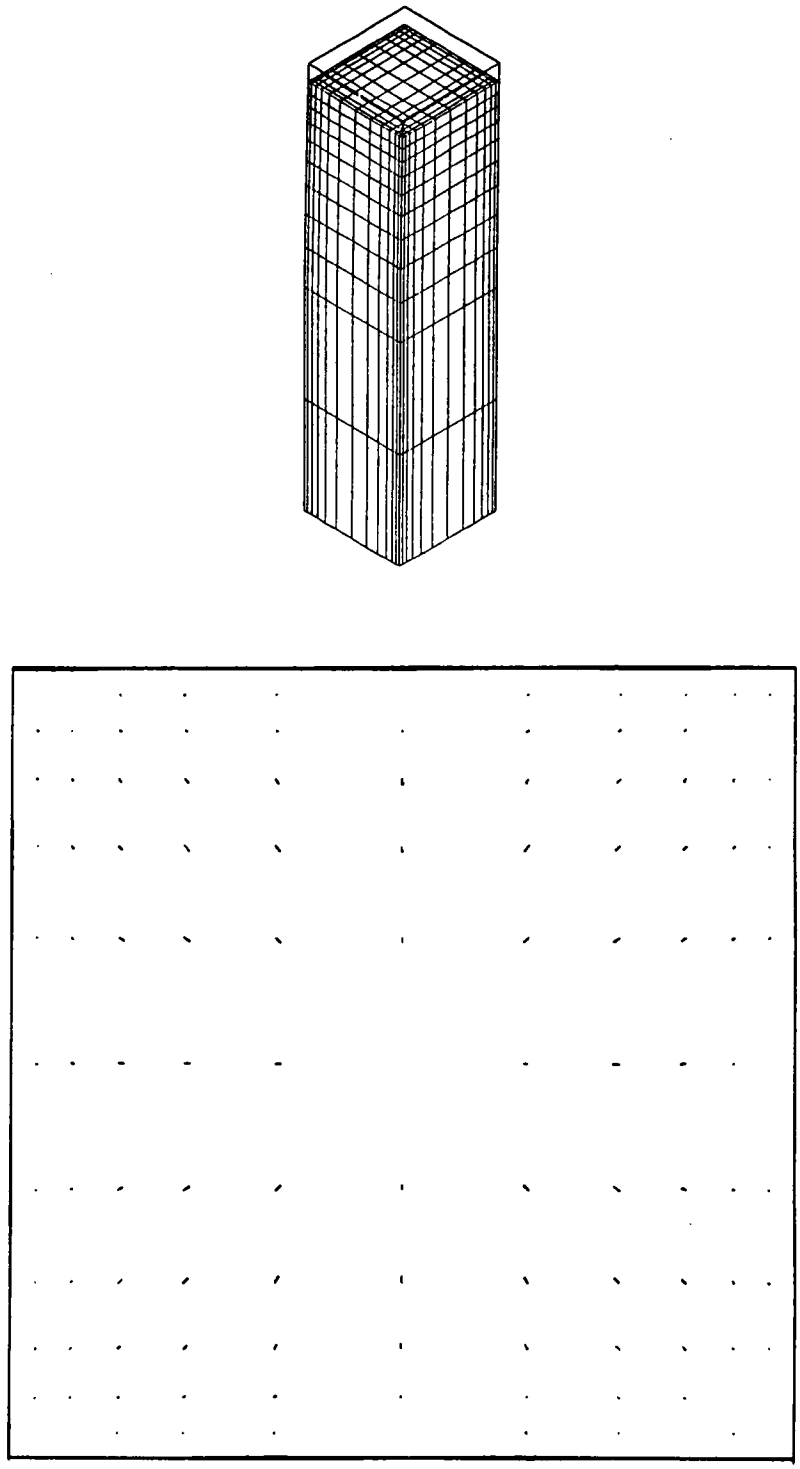


Figure 15. Velocity Vector Pattern For 3-D 1 cm x 1 cm x 4 cm Top Heating Through a .5 cm Diameter Surface - plane #4

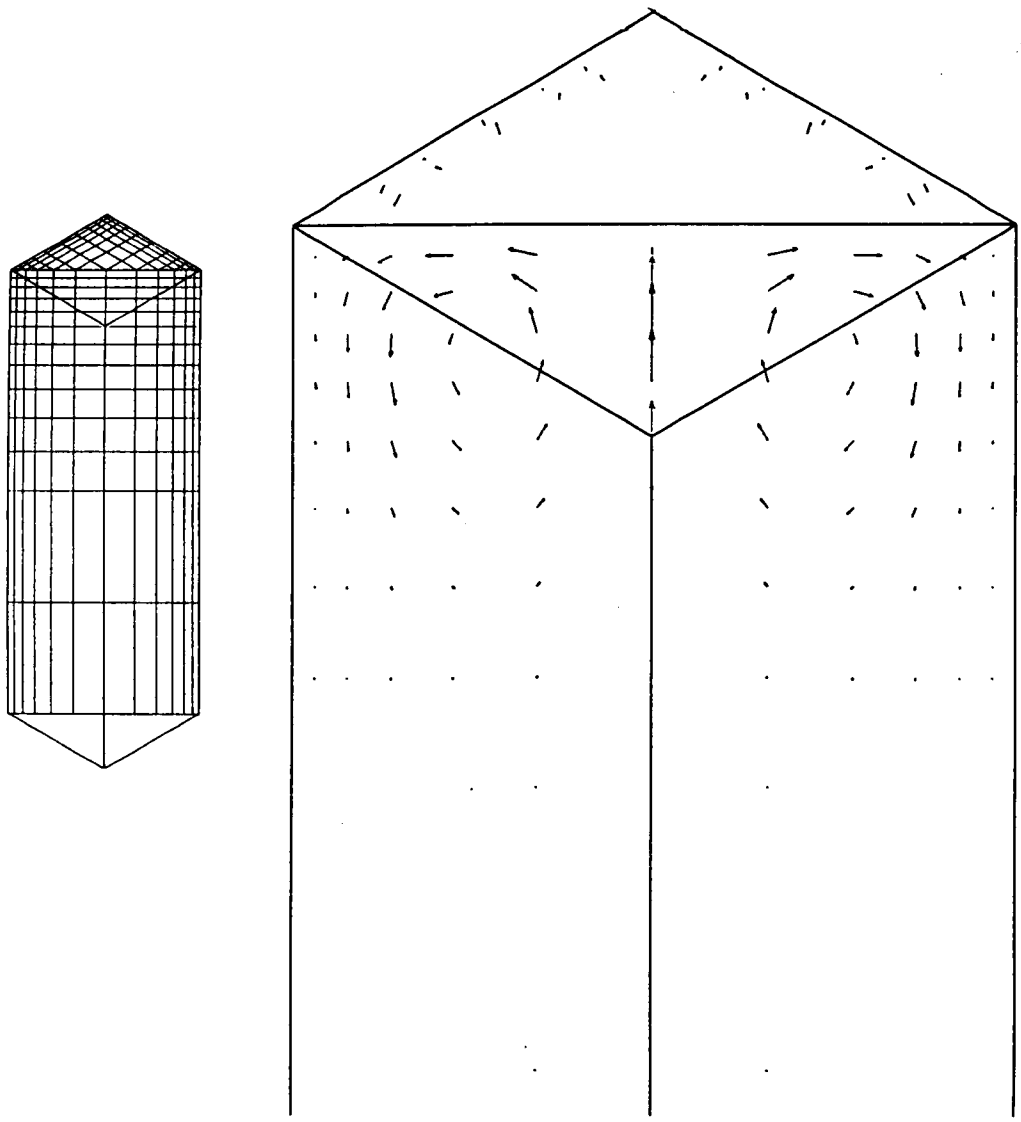


Figure 16. Velocity Vector Pattern For 3-D 1 cm x 1 cm x 4 cm Top Heating Through a .5 cm Diameter Surface - plane #5

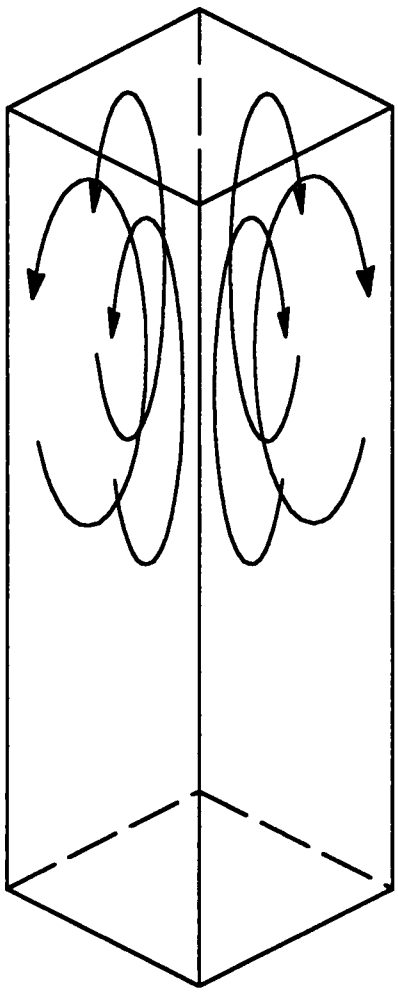


Figure 17. Velocity Vector Pattern For 3-D 1 cm x 1 cm x 4 cm Top Heating Through a .5 cm Diameter Surface - overview

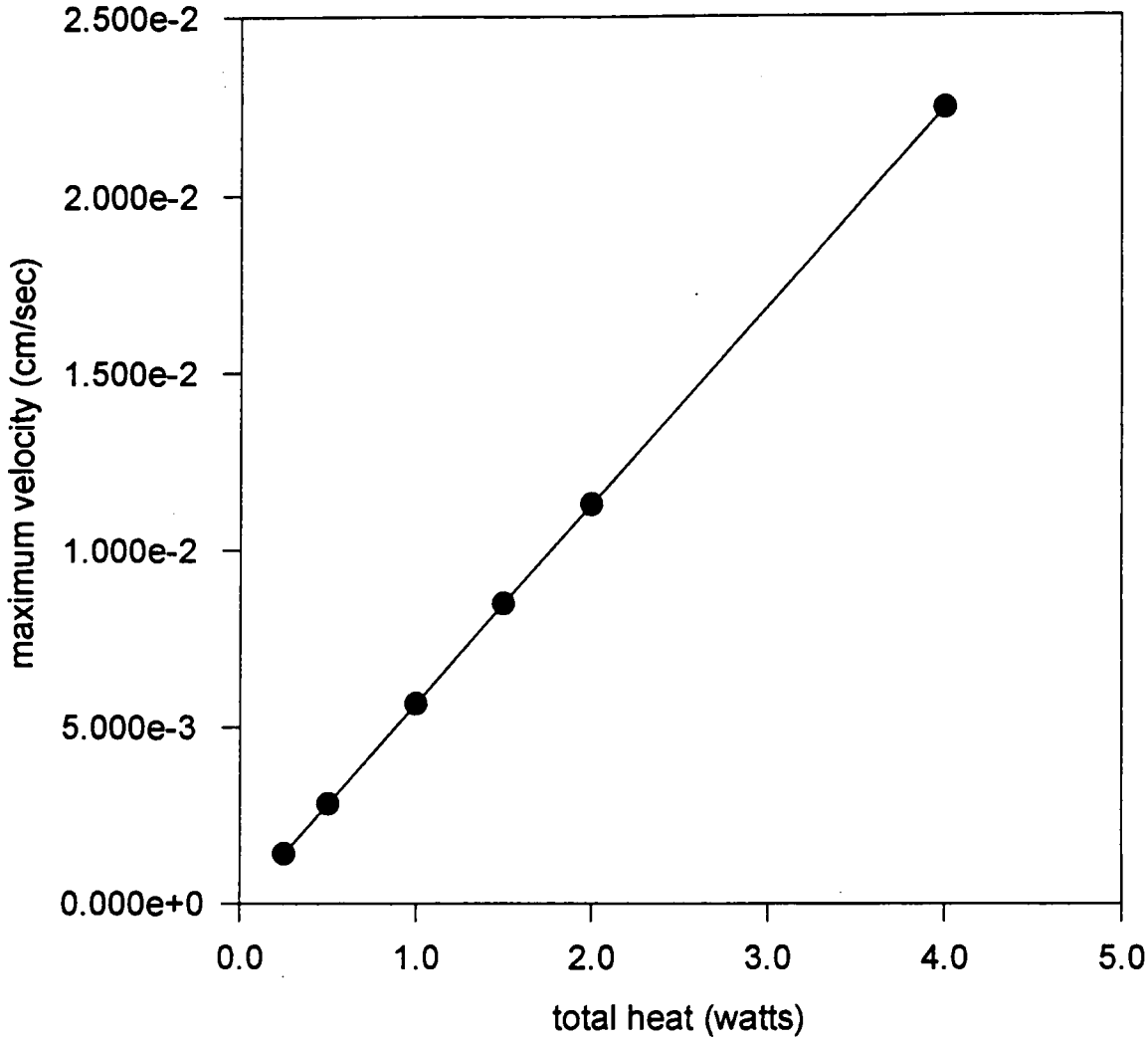


Figure 18. Plot of Total Heat vs. Maximum Velocity for 3-D 1 cm x 1 cm x 4 cm Geometry With Top Heating Through a .5 cm Diameter Surface

THREE DIMENSIONAL SIMULATIONS WITH LENGTHENED AMPULES

A quick series of 3-D simulations would be run. The particular ampules that would be studied here would be similar to those investigated in the previous section, but the lengths in the y-direction would be extended. The lengths of the volumes to be studied were 2.5, 5, 10 and 20 centimeters (see Figure 19). These 3-D simulations were investigated with heated areas on the top, .5 cm wide running the length of the volumes, with a total heat input of 1.00 watt per centimeter (in the y-direction). Note that this is different than the physically applied circularly heated areas of the previous section.

The motivation behind this is to make a comparison between 2-D cross sectional representations of the flowfield across the width of the ampule at its midpoints, and the 2-D 1.00 watt top heating ampule flow field. As the length of these 3-D ampules is increased, the flowfield across the midsection should more closely approximate the 2-D flowfield. If it does not, then the computational model might be flawed and should be suspect.

As the ampule length was increased (more closely approximating that of an infinitely long volume), the cross section representation of the flow field across the width more closely approximates that of a 2-D flow. This is due to the effect of the ends of the volume being more removed.

The 3-D cross sectional maximum velocities are shown in Table 7 and the comparisons of the maximum velocities of the extended ampules to the maximum

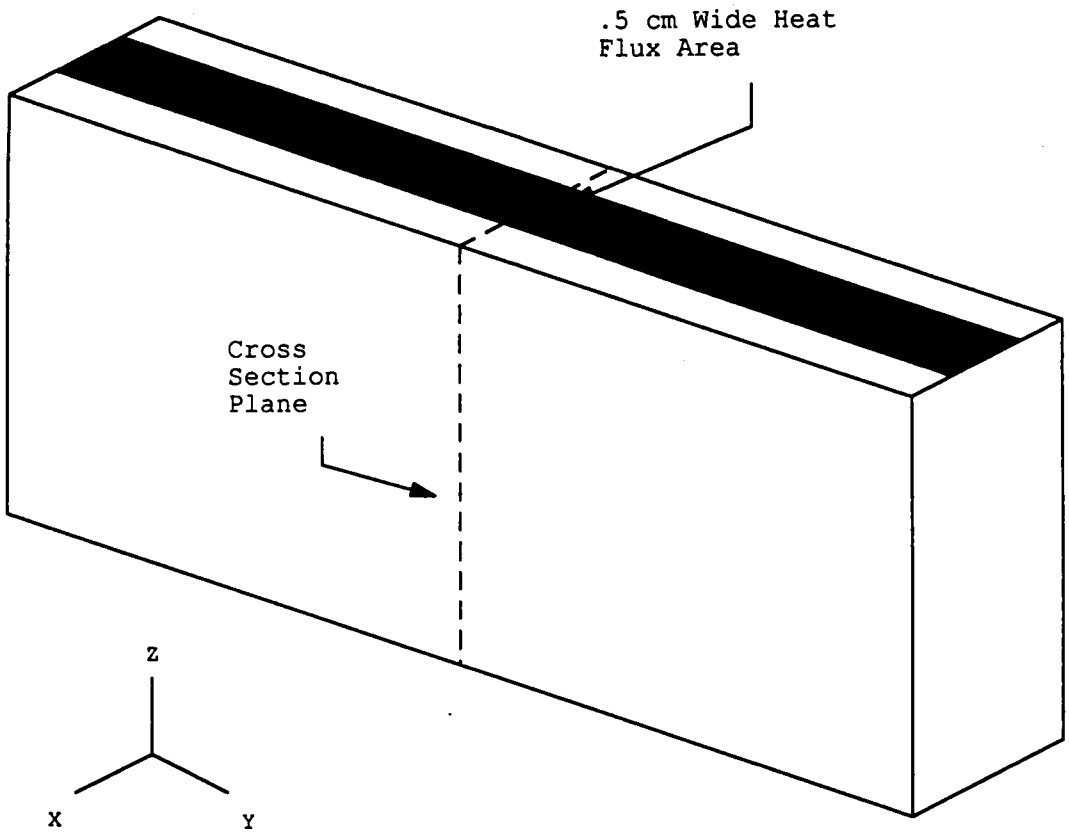


Figure 19. Typical Extended Ampule
1 cm x 4 cm x 10 cm

Table 7. Ampule Length and Maximum Velocities for Coarse and Fine Meshes

Ampule Length (cm)	Coarse Mesh Maximum Velocity (cm/sec)	Fine Mesh Maximum Velocity (cm/sec)
2.5	2.950×10^{-3}	1.359×10^{-3}
5	2.199×10^{-3}	1.211×10^{-3}
10	2.144×10^{-3}	1.197×10^{-3}
20	2.269×10^{-3}	1.187×10^{-3}

velocity of the 2-D, 1.00 watt case are shown graphically in Figure 20. Two sets of trials were run. The first was a mesh consisting of 13 elements high by 12 elements wide by 12 elements long, identical to the mesh geometry of the previous section, simply "stretched" in the Y-dimension. The second was a finer mesh of 13 elements high by 8 elements wide by 18 elements long. The second set of trials were run because the first set of trials did not appear to provide enough resolution in the lengthened axis' direction.

The finer mesh provides a fairly good match to the accepted 2-D value of the maximum velocity. The incorporation of the second set of trials with the finer mesh seems justified in the fact that the velocities calculated here and the 2-D maximum velocities appear more convergent. With confidence in the computational model remaining unshaken, the next set of 3-D simulations continued.

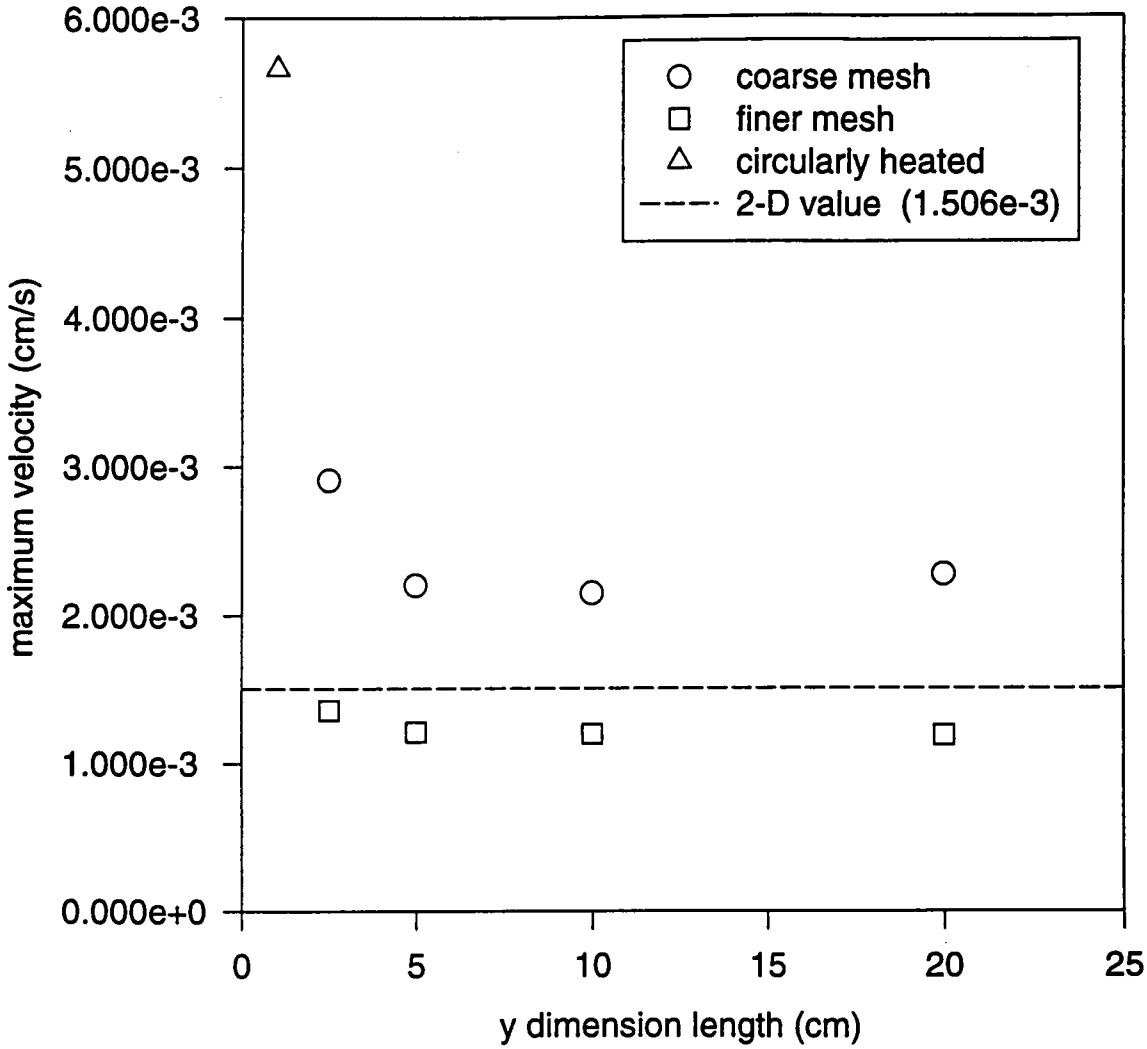


Figure 20. Plot of Maximum Velocity vs. Ampule Length, with 2-D comparison

THREE-DIMENSIONAL SIDE HEATING SIMULATIONS

The 3-D simulations of flow were continued and carried out utilizing another 3-D mesh of 14 elements high by 10 elements wide by 10 elements long, representing the 1 cm x 1 cm x 4 cm ampule. The new mesh was necessitated by the fact that fluid flow could no longer be expected to be confined at the top of the ampule. For these set of trials, the heating surface was a .5 cm diameter area centered on one of the side faces, as shown in Figure 21. It was determined that finer element resolution on the bottom of the ampule was necessary because results from the 2-D cases indicate that a measurable fluid flow may occur there.

The heat inputs were .25, .50, 1.00, 1.50, 2.00, and 4.00 watts. The maximum velocity for each total heat is shown in Table 8. The flow fields are all identical to each other except in scale, as represented by Figures 22 through 27. The maximum velocity for each total heat is plotted in Figure 28.

Table 8. Maximum Velocity for Each Total Heat
Side Heating 3-D - 1 cm x 1 cm x 4 cm

Total Heat (watts)	Maximum velocity (cm/sec)
.25	2.979×10^{-3}
.50	5.958×10^{-3}
1.00	1.190×10^{-2}
1.50	1.790×10^{-2}
2.00	2.380×10^{-2}
4.00	4.760×10^{-2}

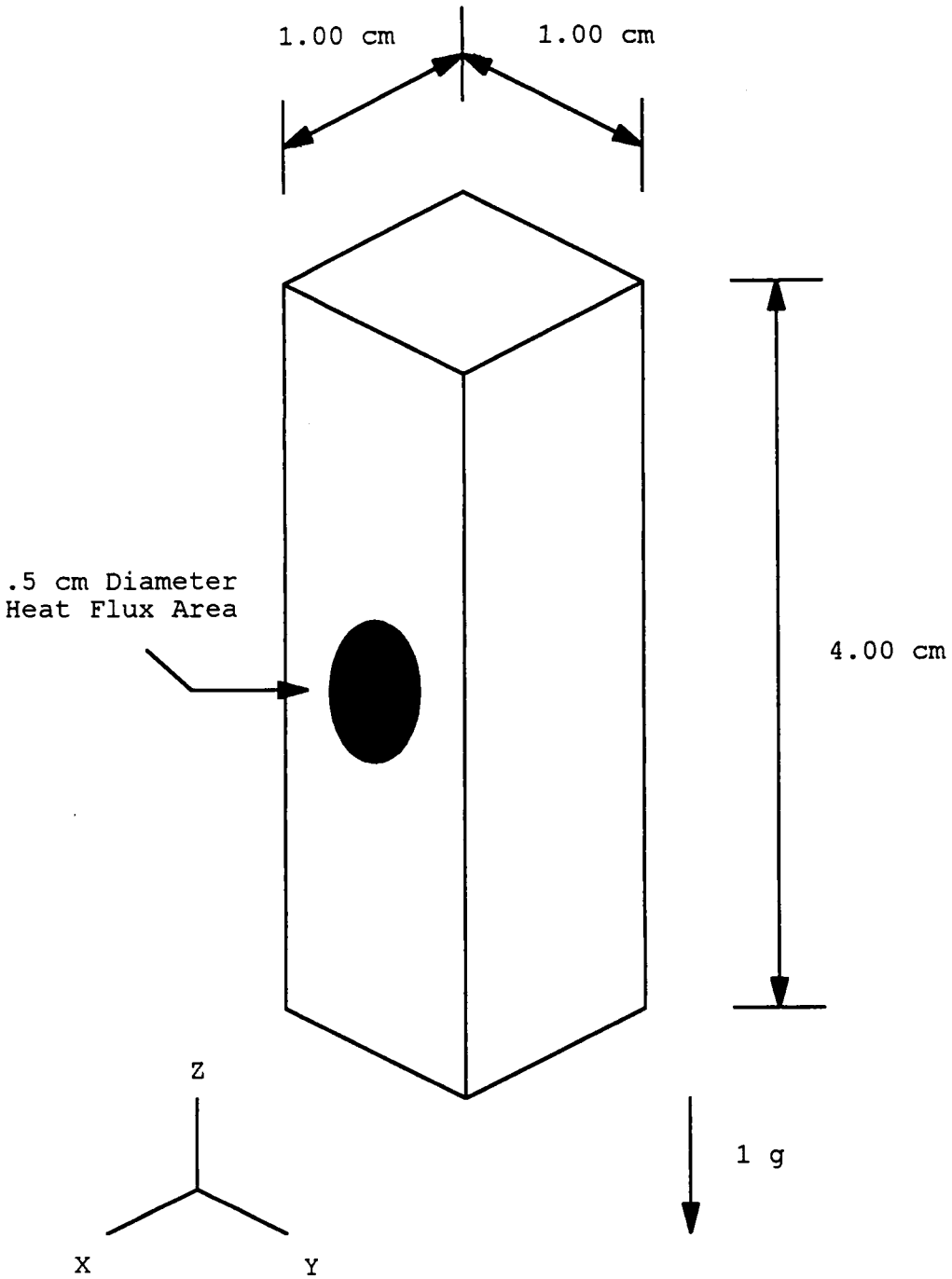


Figure 21. 3-D Side Heating Configuration

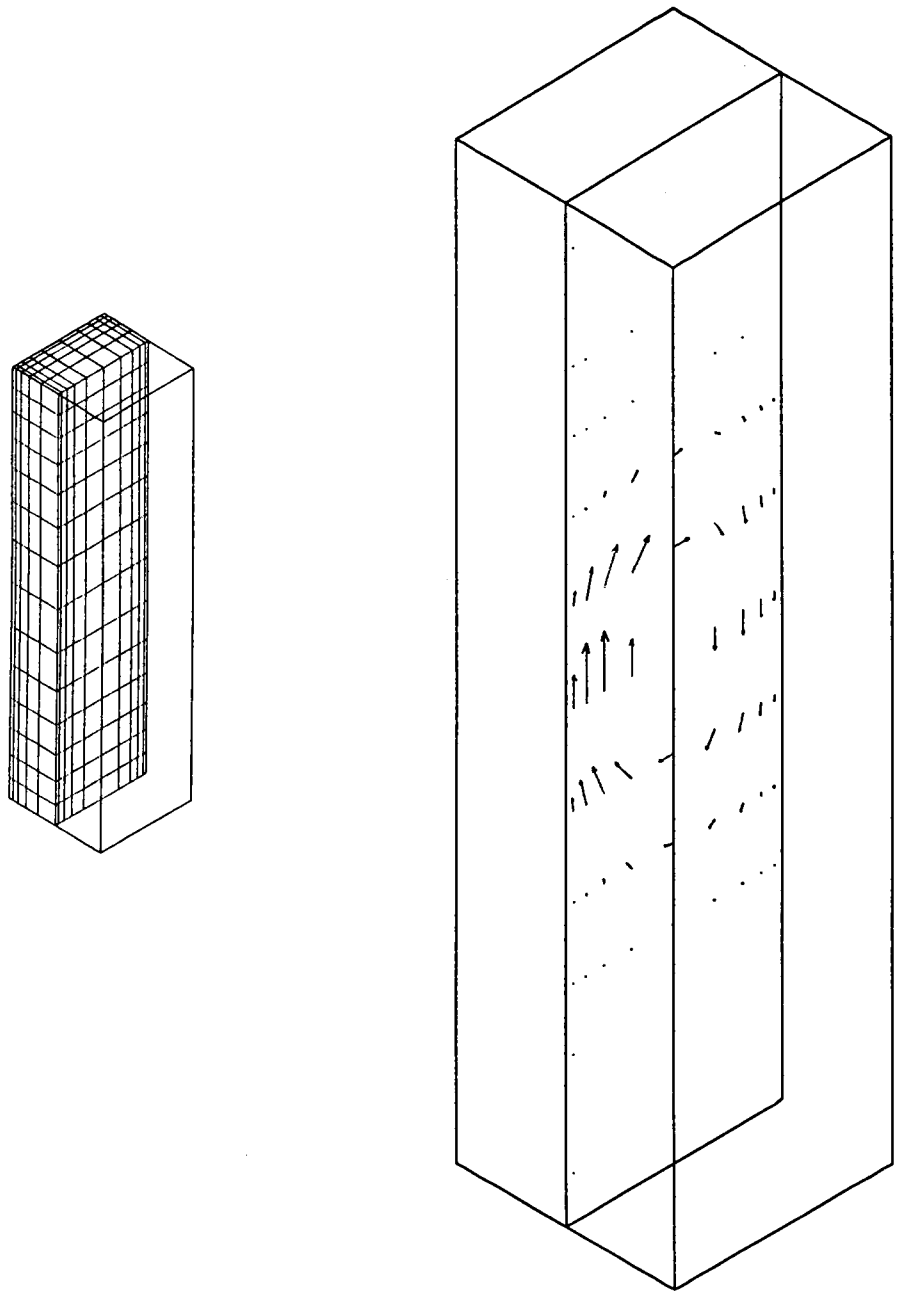


Figure 22. Velocity Vector Pattern For 3-D 1 cm x 1 cm x 4 cm Side Heating Through a .5 cm Diameter Surface - plane #1

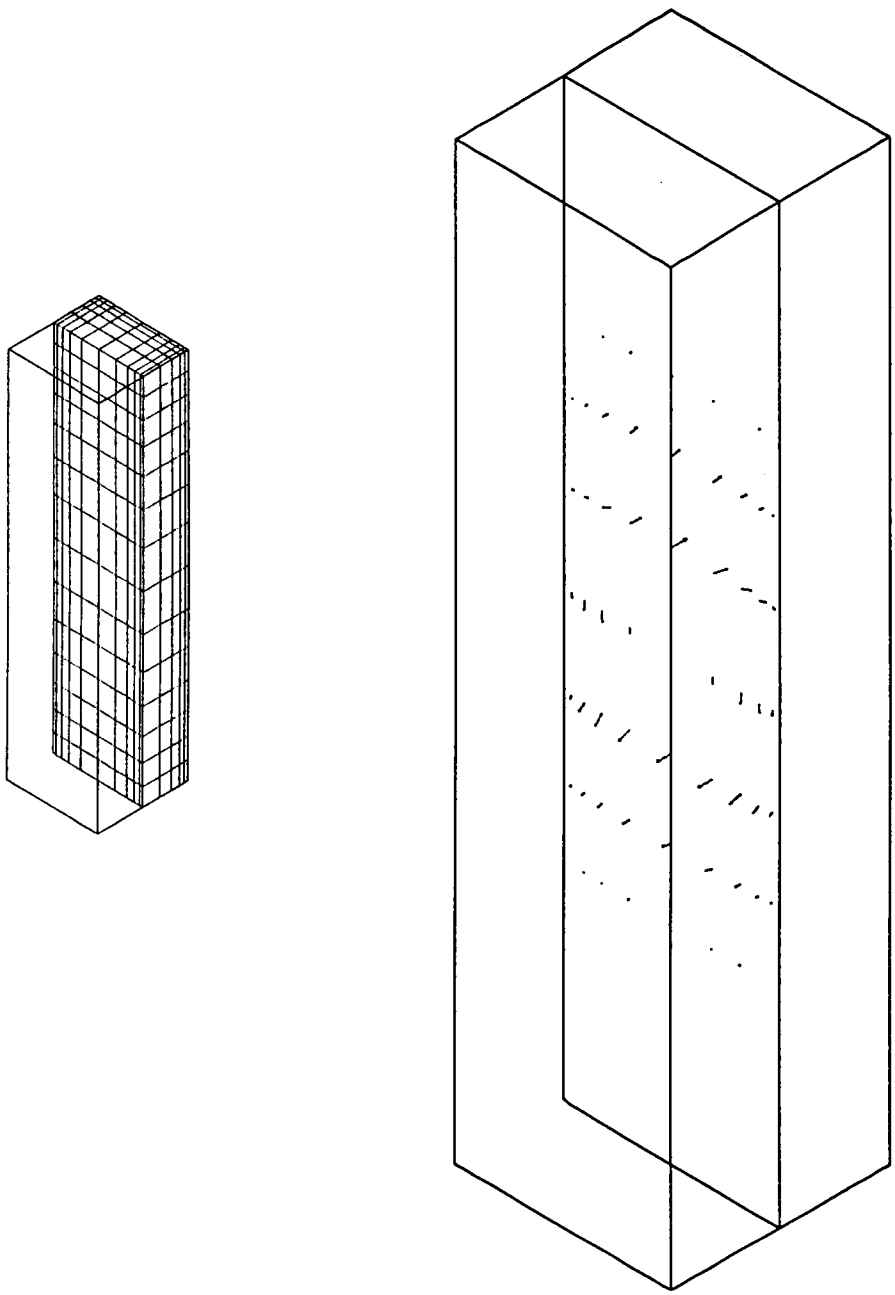


Figure 23. Velocity Vector Pattern For 3-D 1 cm x 1 cm x 4 cm Side Heating Through a .5 cm Diameter Surface - plane #2

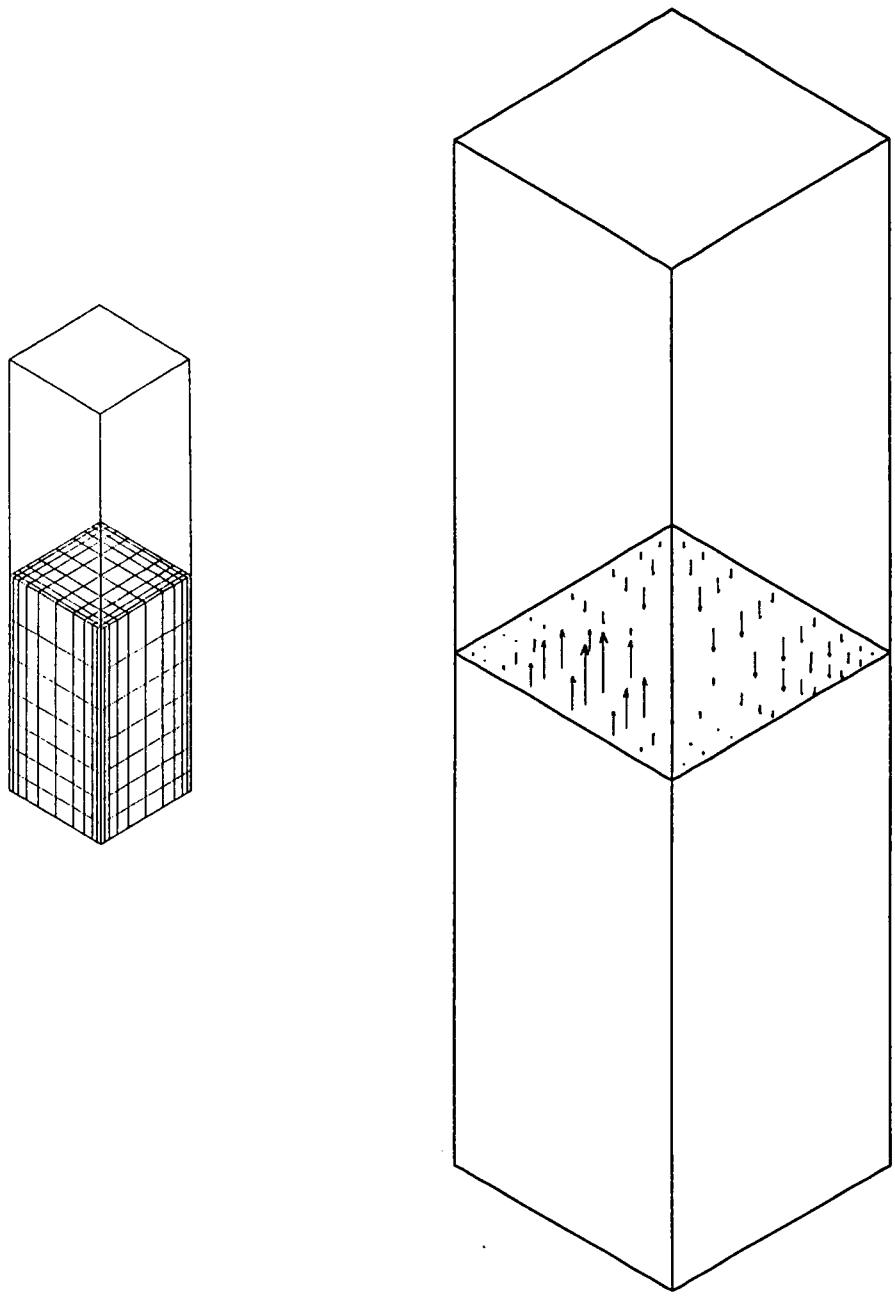


Figure 24. Velocity Vector Pattern For 3-D 1 cm x 1 cm x 4 cm Side Heating Through a .5 cm Diameter Surface - plane #3

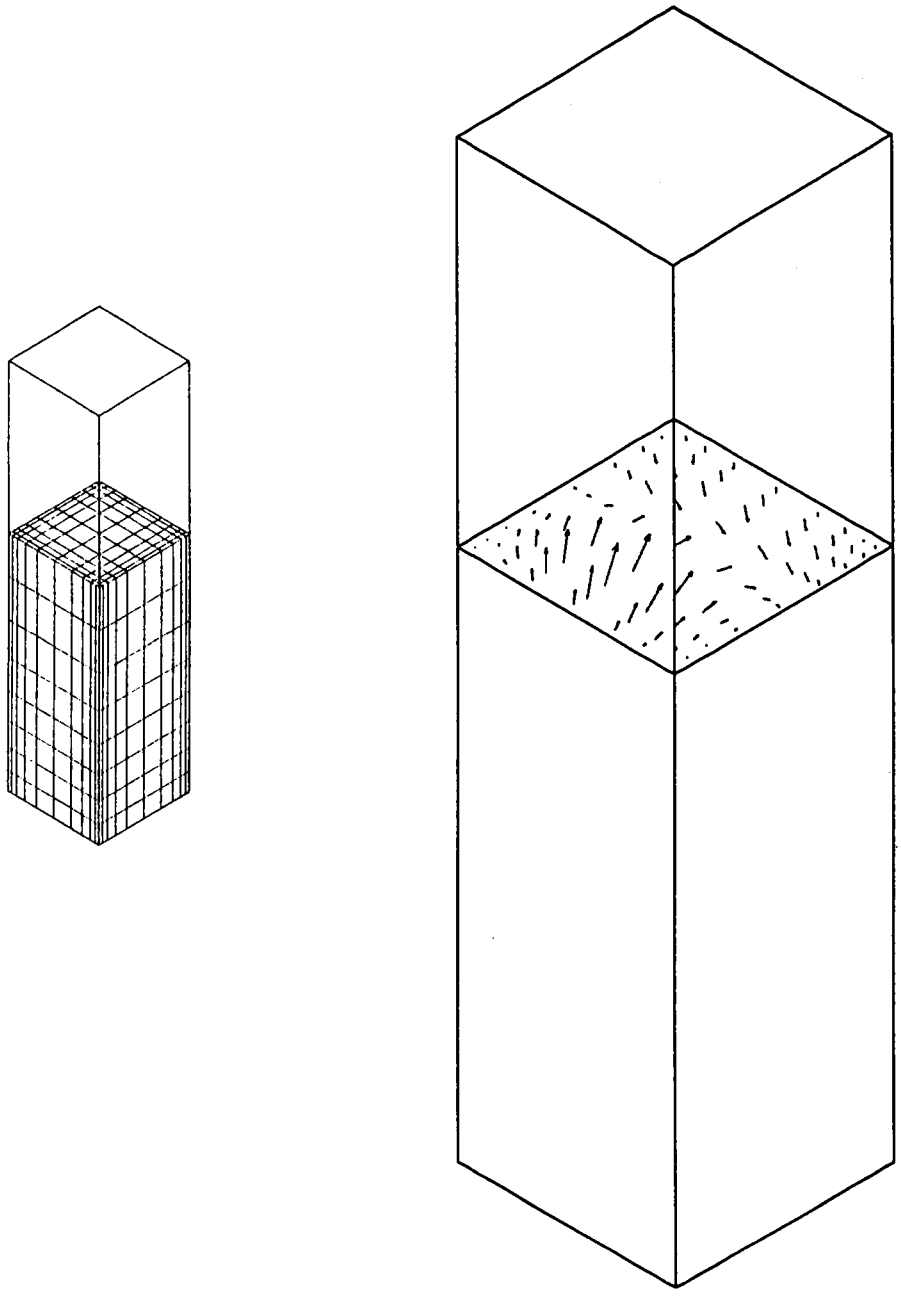


Figure 25. Velocity Vector Pattern For 3-D 1 cm x 1 cm x 4 cm Side Heating Through a .5 cm Diameter Surface - plane #4

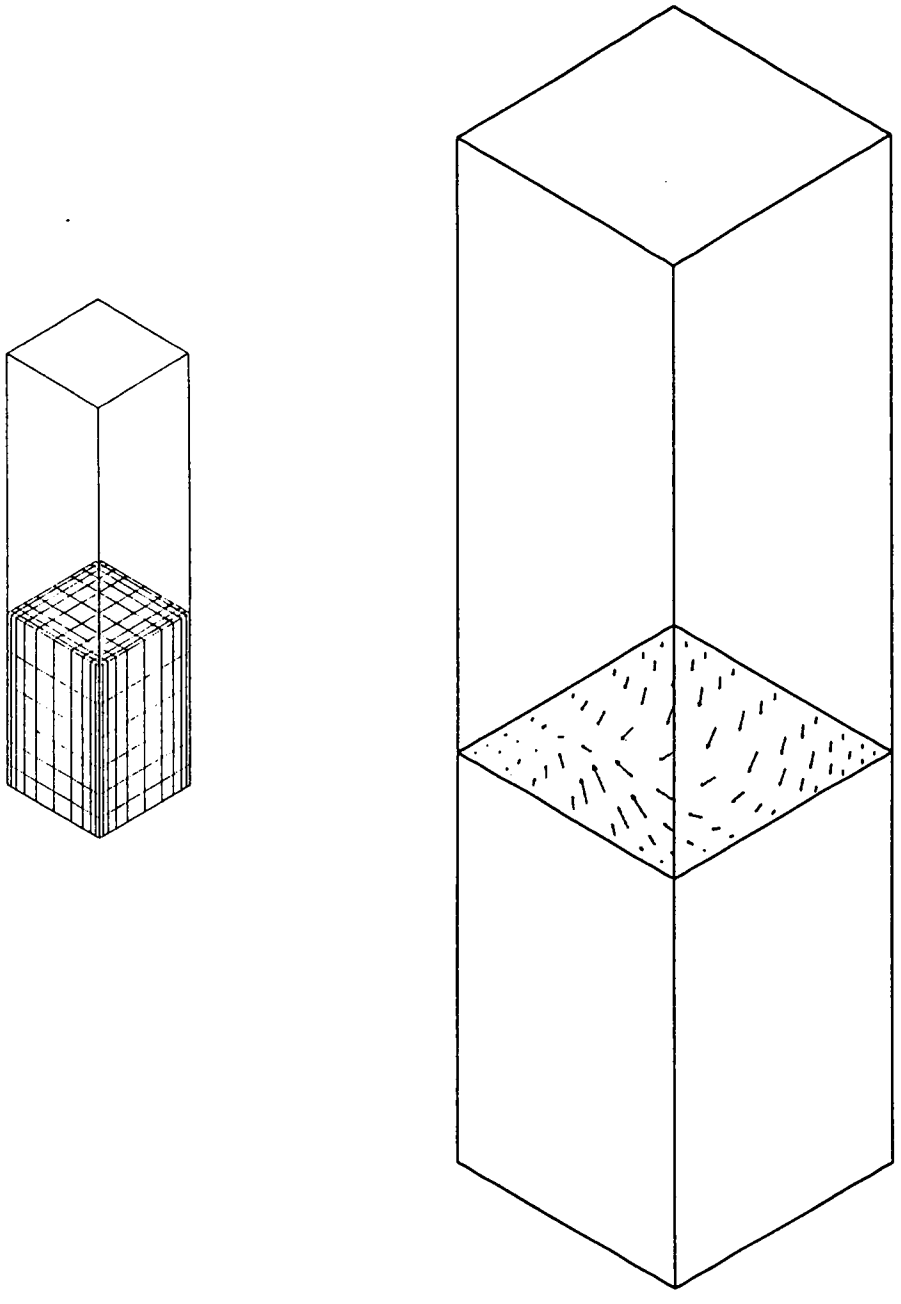


Figure 26. Velocity Vector Pattern For 3-D 1 cm x 1 cm x 4 cm Side Heating Through a .5 cm Diameter Surface - plane #5

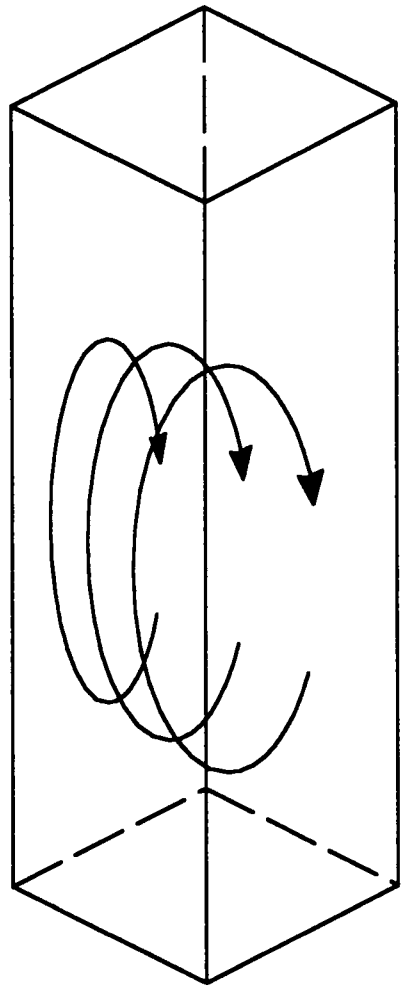


Figure 27. Velocity Vector Pattern For 3-D 1 cm x 1 cm x 4 cm Side Heating Through a .5 cm Diameter Surface - overview

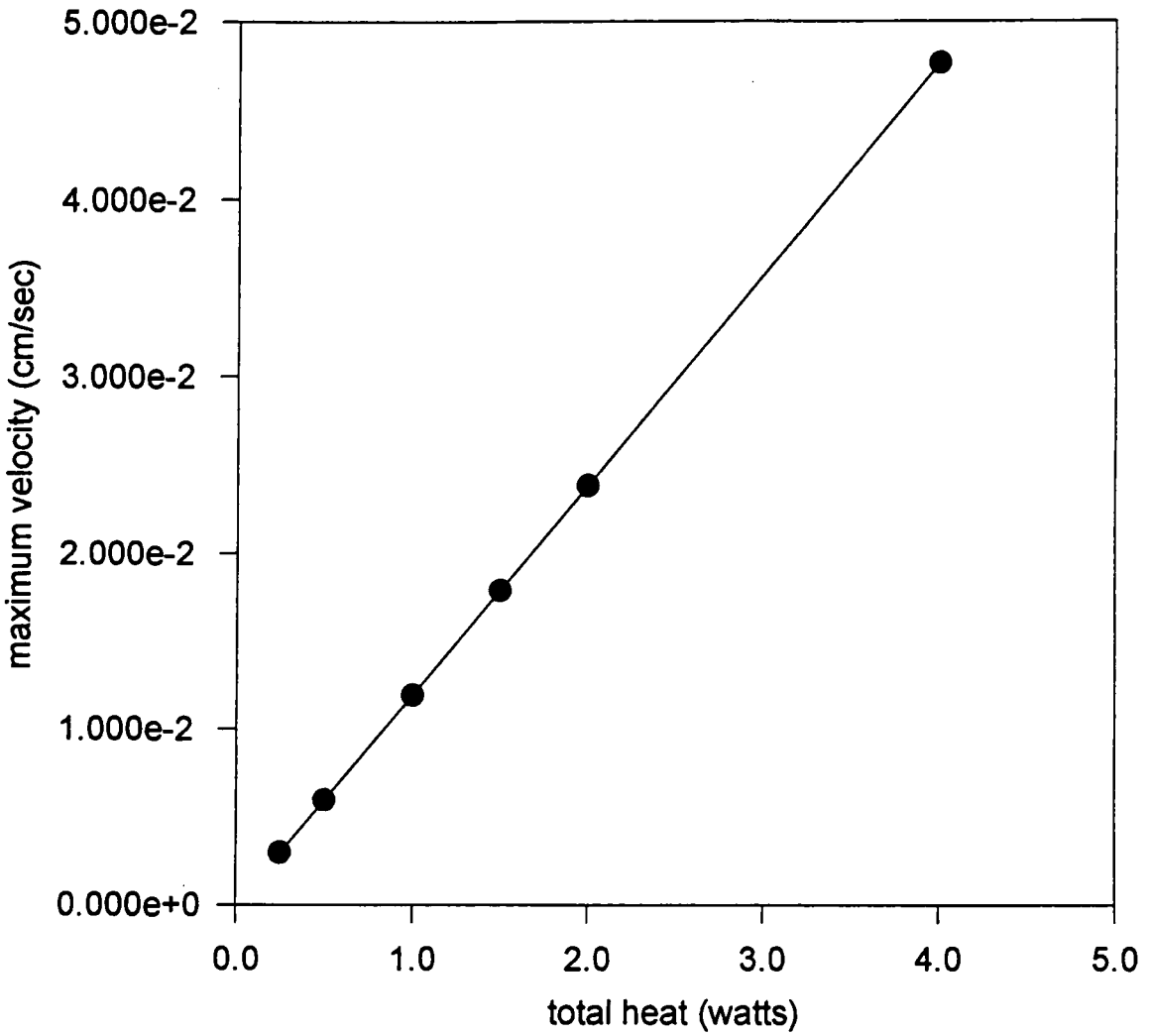


Figure 28. Plot of Total Heat vs. Maximum Velocity for 3-D 1 cm x 1 cm x 4 cm Geometry With Side Heating Through a .5 cm Diameter Surface

The convective patterns of these 3-D flows have the appearance expected based on the 2-D side heating flow patterns previously determined, and the velocities of the flows have reasonable values. A cursory investigation of the 3-D side heating velocities show that they are roughly 8 times greater in magnitude than the 2-D side heating velocities. Again, it is suspected that this could be accounted for by the differences in flux density between the 2-D and 3-D. Here the effect of flux density may be more pronounced than in the top heating 2-D/3-D comparison, because the location of the heating surfaces lend themselves to a more unstable geometry and hence, a greater flow velocity, than in the top heating trials.

REDUCED GRAVITY FLOWFIELD MODELING

The 3-D simulations with the 1 cm x 1 cm x 4 cm ampule with top heating previously solved were solved with gravity vectors pointing downward but with values of 10^{-2} g, 10^{-3} g, and 10^{-4} g. If the 1 g. computational model turns out to match the actual flow parameters determined experimentally, then the results determined in this section will be applied to further research to be carried out in a long duration microgravity environment. The maximum velocities determined for the reduced gravity are shown in Table 9 and plotted, along with the maximum velocities for 1 g, in Figure 29.

Table 9. Maximum Velocities for Each Heat for 10^{-2} g, 10^{-3} g, and 10^{-4} g

Total Heat (watts)	Maximum velocity 10^{-2} g (cm/sec)	Maximum velocity 10^{-3} g (cm/sec)	Maximum velocity 10^{-4} g (cm/sec)
.25	1.420×10^{-5}	1.420×10^{-6}	1.420×10^{-7}
.50	2.839×10^{-5}	2.839×10^{-6}	2.839×10^{-7}
1.00	5.679×10^{-5}	5.679×10^{-6}	5.679×10^{-7}
1.50	8.517×10^{-5}	8.517×10^{-6}	8.517×10^{-7}
2.00	1.136×10^{-4}	1.136×10^{-5}	1.136×10^{-6}
4.00	2.271×10^{-4}	2.271×10^{-5}	2.271×10^{-6}

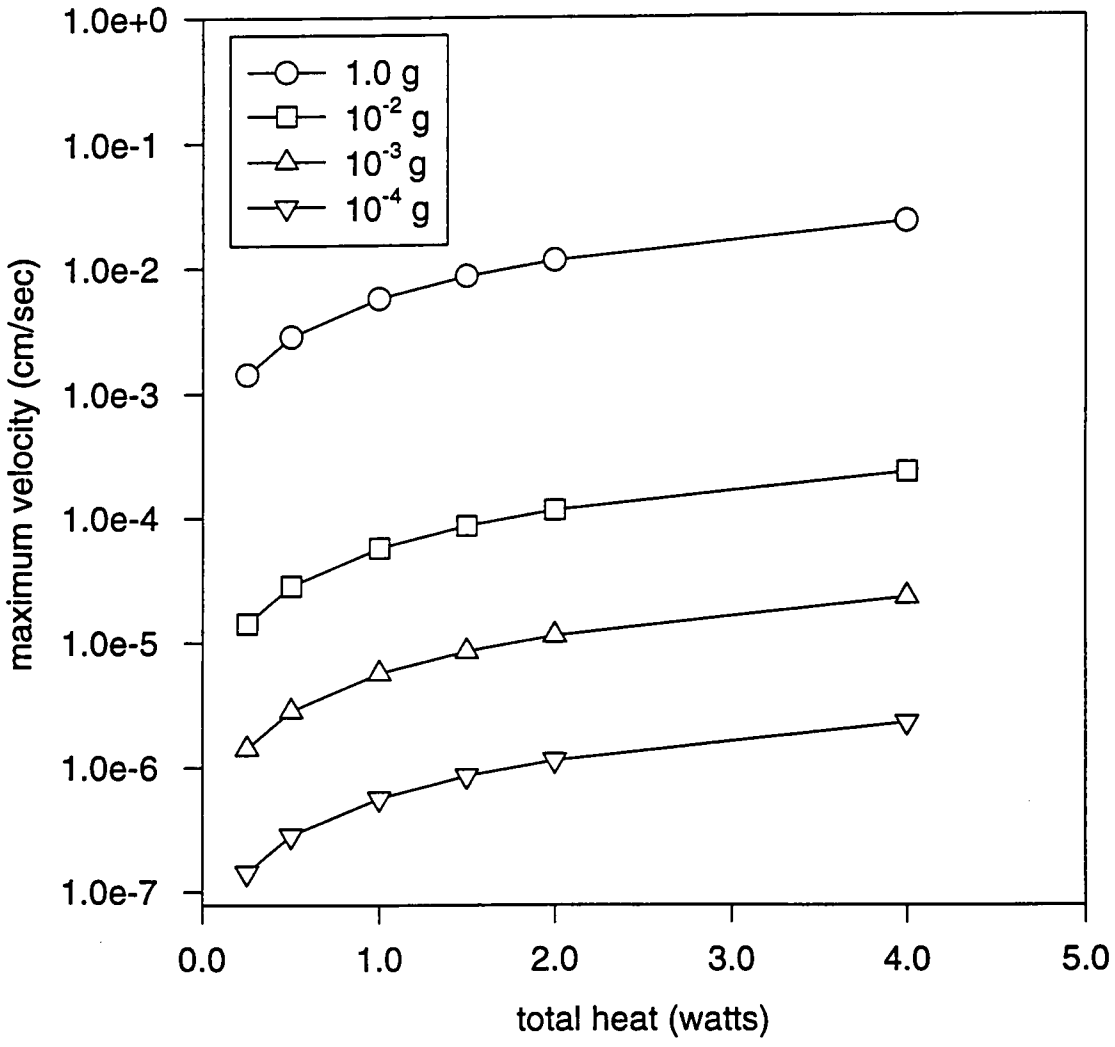


Figure 29. Plot of Total Heat vs. Maximum Velocity for 3-D 1 cm x 1 cm x 4 cm Geometry With Top Heating Through a .5 cm Diameter Surface, 1.0 g, 10^{-2} g, 10^{-3} g, and 10^{-4} g

5. CONCLUSION

Since all of the flows investigated were simulated flows, it was necessary to set criteria for confirmation of the validity of the determined data. The scale of the velocities encountered certainly needed to exhibit reasonable values (no extreme values were permitted). The flows that developed needed to exhibit flow patterns that conform to what we already know about convective flow.

The maximum velocity of any particular trial would be the velocity scale U, and must depend on the gravitational acceleration and the temperature of the system according to:

$$U \propto g(T-T_{\infty}) \qquad [10]$$

where U is the maximum velocity or the velocity scale (Antar and Nuotio-Antar, 1993). Since heat is proportional to temperature, then

$$U \propto gQ \qquad [11]$$

where Q is the total heat (Tipler, 1982).

One of the first characteristics noticeable in all of the plots of maximum velocity versus total heat is the linear relationship between the two. This behavior was expected according to [7] and should it not have occurred, the computational model utilized would have been suspected to be incorrect.

The next item of interest is in Table 9 and Figure 29. Here it is apparent that the maximum velocity is a linear function of the gravitational acceleration, as also predicted by [11] above. This serves as another validity check for the computational model.

This leads to the conclusion that, should the 3-D, 1-g computational model and its corresponding flow patterns produced within this thesis match the corresponding flows observed empirically in a 1-g laboratory, then the predicted flows for the reduced gravity environments would be accurate and representative of how comparable liquids in such containers would behave.

REFERENCES

REFERENCES

1. Antar, Basil N, and Vappu S. Nuotio-Antar. Fundamentals of Low Gravity Fluid Dynamics And Heat Transfer. Boca Raton, FL: CRC Press, Inc., 1993.

2. Cember, Herman. Introduction to Health Physics. New York, NY: Pergamon Press, 1969.

3. Fluid Dynamics International, Inc. FIDAP 7.0, FIMESH User Manual. Evanston, IL.: Fluid Dynamics International, 1993.

4. Fluid Dynamics International, Inc. FIDAP 7.0, FIPOST User Manual. Evanston, IL.: Fluid Dynamics International, 1993.

5. Fluid Dynamics International, Inc. FIDAP 7.0, FIPREP User Manual. Evanston, IL.: Fluid Dynamics International, 1993.

6. Fluid Dynamics International, Inc. FIDAP 7.0, Tutorial Manual. Evanston, IL.: Fluid Dynamics International, 1993.

7. Handbook of Chemistry and Physics. Cleveland, OH: Chemical Rubber Company, 1972.

8. Hung, R. J., and Y. T. Long. "Transient Numerical Simulation of Convection-Driven Flow Field and Temperature Distribution of Vapor Deposition Under Normal and Oblique Gravity Accelerations." (Unpublished paper). 1995

9. "Lasers, Solid State Pulsed." Laser Focus World 1997 Buyers Guide, 15 Dec. 1996, p.184.

10. Mills, D.L., Nonlinear Optics - Basic Concepts. New York, NY: Springer-Verlag, 1991.

11. Mohlmann, G. R., "Perspectives for Non-linear Polymers in Electro-optic Applications," Organic Materials for Non-linear Optics (London: The Royal Society of Chemistry, 1989), p. 275.

12. Paley, Mark S., Basil N. Antar, Yeon-Taik Kim, Donald O. Frazier, and Bill Witherow. "Gravitational Effects on the Morphology and Kinetics of Photo-Deposition of Polydiacetylene Thin Films from Monomer Solution." (Unpublished paper). 1995.

13. Tipler, Paul A. Physics. Rochester, MI: Worth Publishers, 1982.

APPENDIX

There are few instructions in a FIDAP source file that actually need more than a cursory explanation to understanding their functioning. The following presentation describes the statements and their functions in detail, for the typical FIDAP source file that immediately follows. In this case , the source file is for the top heating, 1.00 watt 3-D trial.

TITLE - the line immediately following the TITLE statement is the text string that will appear on all plots generated during the FIPOST post processing analysis program.

FIMESH - invokes the FIMESH subprogram, and defines this problem as 3-dimensional with minimum mesh size of 9, as well as maximum Integer Space coordinate values of 9 in the I, J, and K directions in FIDAP's Integer Space (corresponding to X, Y and Z physical directions).

EXPI, EXPJ, EXPK - the line immediately following these statements allows control of mesh density. In the case of the EXPI statement and the line immediately following, the number of places for numbers is 9 (corresponding to the 9 described by the FIMESH statement). As an example, let us look at place number 6. The number 10 occupies this position. This implies that while we have defined a mesh in Integer Space of 9 by 9 by 9, the line following the EXPI statement has assigned an actual finite element node density of 13 (mesh density of 13 minus 1, or 12 elements) in the I direction, and the original node 6 in integer space is now, node 10 in the real geometry of the simulation.

POINT - the next 25 lines following point describe the exact locations of points of major importance (such as corners, edge midponts, points used for defining the heating surfaces).

There are 7 numbers per point definition. The first digit is an integer and is the point's ordinal number assignment; just a label, nothing else. The next three numbers are integers and refer to the Integer Space I, J, and K coordinates of the point. The final three numbers are the geometric real space X, Y, and Z coordinates

LINE - the statements following the LINE statement define significant lines in the problem's geometry. The first digit identifies the point at which the line begins, the second identifies the point at which the line terminates. The third number identifies the ratio of the last line segment between nodal points to the first line segment between nodal points on the line just defined. The fourth number identifies the algorithm used to determine the ratio scheme; here 3 designates the ratio of the last segment to first segment.

ARC - the statements following the ARC statement draw arcs starting at the point the first number identifies and ending at the point the second number identifies, centered on the point the third number identifies.

SURFACE - and the subsequent statements define the outer boundaries, one 2-D panel at a time. They were identified by a diagonal spanning the 2-D face.

3-D - and the following statement define the 3-D volume by a diagonal running through the volume.

NUMBER - indicates in which order FIDAP processes coordinates in calculations (not in which order they are listed). This is a necessary but inconsequential instruction for these simulations, but the instruction has use when the order in which coordinates are used in calculations needs to be controlled.

ELEMENTS - this first ELEMENTS statement determines the finite element geometries. In this case, brick shaped objects are chosen, the print option for later display is chosen, the number of nodes, 8, representing one node on each vertex of each "brick" element is chosen, and a name for the elements as a collective whole, "fluid," is chosen. The numbers 1 17 on the next line define the 3-D region the ELEMENTS statement applies to (similar to the 3-D statement listed above).

ELEMENTS - this second ELEMENTS statement defines the boundaries of the physical problem and assigns the name "wall" to the collective whole. The Boundary faces are defined by a diagonal spanning each face on all sides (except for the heating surface area.)

ELEMENTS - the third ELEMENTS statement defines the heating surface, called "hotwall."

END - ends the FIMESH subprogram and returns control to the main root command program FIDAP.

FIPREP - invokes the FIPREP subprogram and begins its execution

PROBLEM - defines the particular problem. BUOYANCY and NONLINEAR make inclusive, all nonlinear and buoyancy terms in the momentum equation.

PRESSURE - this statement specifies the approach to the problem, in this case, discontinuous pressure discretization.

SPECIFICHEAT - specifies the specific heat of the fluid, in this case, a CONSTANT value throughout the fluid of .99795 cal/gm-^{0}C.

VISCOSITY - specifies the viscosity of the fluid, in this case, a CONSTANT value of .008904 Poise.

VOLUMEX - specifies the volume expansion coefficient, in this case, a CONSTANT value of 1.1204 x 10^{-4}/^{0}C.

CONDUCTIVITY - specifies the heat conductivity, in this case, a CONSTANT value of .0014503 cal/cm-sec-^{0}C for the element SET known as "fluid" which is the only element set being used for this problem.

GRAVITY - specifies the gravityacceleration vector direction and magnitude, in this case, downward and parallel to the local vertical with a value of 980 cm/sec^2.

EXECUTION - defines the execution parameters. NEWJOB makes each execution a new, start from the beginning simulation (as opposed to a continuation of a previously partially solved simulation).it appears,

SOLUTION - in this statement, N.R.=7 invokes a Newton-Raphson solution technique with a maximum of 7 iterations before termination without convergence. VELCONV=.001 is the velocity convergence tolerance, RESCONV=.001 is the residual vector convergence tolerance. Iterations are performed until the maximum

number of iterations is reached (as defined in n.r.=7) or until the velocity and residual vector convergence tolerances are reached.

STRATEGY - this statement,, S.S.=1 defines a successive substitution strategy on each iteration.

DENSITY - specifies the fluid density, in this case, .99705 gm/cm^3 throughout the fluid a the start of the execution.

DATAPRINT - specifies output parameters of the solution (or the conditions if iteration limit with no convergence is reached). NORMAL specifies detailed output of input data. PAGE specifies a new page for each output section. NODES specifies printout of nodal coordinates.

POSTPROCESS - this statement specifies when the various solution quantities are output to the results database file. In this case, results are output at each iteration.

ENTITY - these first of these statements defines the collection of elements named "fluid" with the attributes of a FLUID. The second ENTITY statement plots the boundaries from the collection of surfaces of the fluid elements, and names these surface elements "wall." The third of these statements does the same as the second of these statements, but for the area on the wall representing the heated surface and named "hotwall."

RENUMBER - optimally renumbers the nodes of the mesh so as to minimize the profile of the coefficient matrix. This streamlines the execution of the simulation.

BCNODE - these three statements apply boundary conditions directly. The first two BCNODE statements specify a zero velocity (no slip) condition at the walls of the container, the walls being made up of the entity "wall" (representing the container's wall except for the heated surface), and the entity "hotwall" (representing the heated surface. The third BCNODE statement specifies a 25 ^{0}C condition on the wall at all surfaces except for the surface representing the heated surface.

BCFLUX - this statement is used to define a flux type boundary condition, in this case, a heat flux across the entity known as "hotwall." The flux has a value of 1.2168 cal/sec-cm^2.

RENUMBER - performs same function as before, except this time incorporating the changes induced by the boundary conditions.

END - ends the FIPREP subprogram and returns control to the main root command program FIDAP.

CREATE - prepares the complete source file for execution in the FISOLV solving portion of the FIDAP root command program.

```
TITLE
1cm x 1cm x 4cm/ .5cm top heat inlet/ 1.00 Watts
FIMESH(3-D,IMAX=9,JMAX=9,KMAX=9)
EXPI
1 0 0 4 7 10 0 0 13
EXPJ
1 0 0 4 7 10 0 0 13
EXPK
1 0 0 0 3 0 0 0 14
POINT
1 1 1 1 0. 0. 0.
2 5 1 1 .5 0. 0.
3 9 1 1 1. 0. 0.
4 9 5 1 1. .5 0.
5 9 9 1 1. 1. 0.
6 5 9 1 .5 1. 0.
7 1 9 1 0. 1. 0.
8 1 5 1 0. .5 0.
9 1 1 5 0. 0. 2.
10 9 1 5 1. 0. 2.
11 9 9 5 1. 1. 2.
12 1 9 5 0. 1. 2.
13 1 1 9 0. 0. 4.
14 5 1 9 .5 0. 4.
15 9 1 9 1. 0. 4.
16 9 5 9 1. .5 4.
17 9 9 9 1. 1. 4.
18 5 9 9 .5 1. 4.
19 1 9 9 0. 1. 4.
20 1 5 9 0. .5 4.
21 5 5 9 .5 .5 4.
22 4 4 9 .25 .25 4.
23 4 6 9 .25 .75 4.
24 6 6 9 .75 .75 4.
25 6 4 9 .75 .25 4.
LINE
1 2 5. 3
3 2 5. 3
3 4 5. 3
5 4 5. 3
5 6 5. 3
7 6 5. 3
7 8 5. 3
1 8 5. 3
1 9 1. 0
13 9 5. 3
```

```
3 10 1. 0
15 10 5. 3
5 11 1. 0
17 11 5. 3
7 12 1. 0
19 12 5. 3
13 14 5. 3
15 14 5. 3
15 16 5. 3
17 16 5. 3
17 18 5. 3
19 18 5. 3
19 20 5. 3
13 20 5. 3
ARC
22 23 21
23 24 21
24 25 21
25 22 21
SURFACE
1 5
1 15
1 19
5 15
5 19
15 19
3-D
1 17
NUMBER
2 1 3
ELEMENTS(BRICK,PRINT,NODES=8,ENTITY="fluid")
1 17
ELEMENTS(BOUNDARY,FACE,ENTITY="wall")
1 5
1 15
1 19
5 15
5 19
13 22
15 25
17 24
19 23
ELEMENTS(BOUNDARY,FACE,ENTITY="hotwall")
22 24
END
```

```
FIPREP
PROBLEM(NONLINEAR,BUOYANCY,3-D)
PRESSURE(PENALTY=1.E-8,DISCONTINUOUS)
SPECIFICHEAT(CONSTANT=.99795)
VISCOSITY(CONSTANT=.008904)
VOLUMEX(CONSTANT=1.1204e-4)
CONDUCTIVITY(SET="fluid",CONSTANT=.0014503)
GRAVITY(MAGNITUDE=980,THETA=0)
EXECUTION(NEWJOB)
SOLUTION(N.R.=7,VELCONV=.001,RESCONV=.001)
STRATEGY(S.S.=1)
DENSITY(CONSTANT=.99705)
DATAPRINT(NORMAL,PAGE,NODES)
POSTPROCESS
ENTITY(FLUID,NAME="fluid")
ENTITY(PLOT,NAME="wall")
ENTITY(PLOT,NAME="hotwall")
RENUMBER(PROFILE)
BCNODE(VELOCITY,ZERO,ENTITY="wall")
BCNODE(VELOCITY,ZERO,ENTITY="hotwall")
BCNODE(TEMPERATURE,CONSTANT=25.,ENTITY="wall")
BCFLUX(HEAT,ENTITY="hotwall",CONSTANT=1.2168)
RENUMBER(PROFILE)
END
CREATE(FISOLV)
```

VITA

Gregory James Gosian was born in Albany, New York on October 16, 1959. He had an early exposure to higher education through his mother, Dr. A. Nancy Avakian, university administrator.

He had a premier education in one of New York State's most well funded school districts in Brighton, NY. His college career took him to Colorado where he received his Bachelor's Degree in Physics and Mathematics in May of 1987 from the University of Colorado at Boulder. During his college years, he was able to satiate his interest in space and fund his education by working at Denver's Gates Planetarium where he wrote astronomy shows, produced exhibits utilizing NASA artifacts, and developed special effects devices for the productions. He then went to Los Angeles, California where he started a successful entrepreneurial venture, L.A. Laser Light, a laser technology firm.

His wish to further his education brought him to UTSI in January of 1995. His interest in aviation and space, and desire to pursue a position with NASA, has kept him a skydiver and experimental aircraft builder. In June of 1996 he met Jacquelyn Sue Dolin as a matter of incredible good fortune. They plan to marry and move to Denver, where the author will assume a position with Lockheed Martin Astronautics.